STRETCHING THE FLEXIBLE MYOSIN II SUBFRAGMENT USING THE NOVEL GRAVITATIONAL FORCE SPECTROSCOPE, AND THE UNCOILING OF S2

James W. Dunn

Thesis Prepared for the Degree of

MASTER OF SCIENCE

UNIVERSITY OF NORTH TEXAS

May 2010

APPROVED:

Douglas D. Root, Major Professor
Robert C. Benjamin, Committee Member
Gerard O'Donovan, Committee Member
Art J. Goven, Chair of the Department of Biological Sciences
Michael Monticino, Dean of the Robert B. Toulouse School of Graduate Studies

Dunn, James W. Stretching the Flexible Myosin II Subfragment Using the Novel Gravitational Force Spectroscope, and the Uncoiling of S2. Master of Science (Biochemistry), May 2010, 65 pp., 4 tables, 14 figures, references, 41 titles.

Familial Hypertrophic cardiomyopathy (HCM) causes ventricle walls to thicken and often leads to sudden death especially in adults. Mutations in the subfragment 2 (S2) of β-cardiac myosin are implicated in the genetic disorder. This S2 region is a coiled-coil rod region resulting from the dimeric form of myosin II. It has been proposed that an elastic quality allows normal S2 to absorb force during the powerstroke according to the sliding filament model. To test the flexibility of single molecules of S2 against levels of physiological force, the Gravitational Force Spectrometer (GFS) is being developed. This novel system employs a standard microscope on an equatorial mount that allows the spectrometer to be rotated freely in space. Stationary glass beads are attached to a microscope slide where the molecule is tethered between the stationary bead and a smaller mobile bead. The GFS is oriented so that the force of gravity can act on the mobile bead and so impart a small force to the tethered subfragment. Additionally, a video system in conjunction with ImageJ software makes a distance measurement of the molecule possible with a resolution of around 11 nm. The S2 can be stretched parallel or perpendicular to the coiled coil to elucidate different structural properties of the rod. This study is the first to show structural evidence that S2 in vertebrate skeletal myosin uncoils proportionally to physiological force loads. Because of this, the usefulness and promise of the novel GFS is highlighted, and the biological role of S2's flexibility can be directly commented on. If the dimer undergoes uncoiling at physiological force loads as shown, then it is reasonable to think that this might occur in nature in response to the stress of the powerstroke on a single molecule. This unwinding could be to absorb force as a mechanism to protect the muscle fiber.

ACKNOWLEDGEMENTS

I would like to acknowledge the undying support of my mentor and major professor, Dr. Douglas Root. The herein work could not be accomplished without his purposeful vision, his deep insights, and his joyful and patient encouragement. I would also like to thank my family whose support has been as vital.

This material is based upon work supported by the National Science Foundation under Grant No. 0842736.

TABLE OF CONTENTS

LIST OF TABLES

LIST OF ILLUSTRATIONS

Figure Page

LIST OF ABBREVIATIONS

AA	Amino acid
ADP	Adenosine diphosphate
AFM	Atomic force microscope
arg-gln	Arginine—glutamine
ATP	Adenosine triphosphate
β-MHC	Beta cardiac myosin heavy chain
bp	Base pair
C1	Initial concentration
C2	Concentration as in C1 V1 = C2 V2
Ca^{2+}	Calcium ion
CL	Confidence level
d	Density
d_{max}	Maximum distance
d_{min}	Minimum distance
DNA	Deoxyriboise nucleic acid
ds	Double stranded
E	Glutamate
E924K	Substitute lysine for glutamate at AA 924
ELC	Essential light chain
F	Force
FRET	Fluorescent resonance energy transfer

g	Gravity
g/cm3	Grams per centimeter cubed
GFS	Gravitaional force spectrometer
HCM	Hypertrophic cardiomyopathy
HMM	Heavy meromyosin
KCl	Potassium chloride
LMM	Light meromyosin
Leu-Val	Leucine--valine
M	Molar
$MgCl_2$	Magnesium chloride
mM	Millimolar
ms	Millisecond
MyBP-C	Myosin binding protein-C
NA	Numerical aperture
na	Not applicable
NIH	National Institutes of Health
nm	Nanometer
OT	Optical trap
PC	Personal computer
pN	Piconewton
R	Rise phase
ra	Radius of mobile bead
rb	Radius of stationary bead

RET	Resonance energy transfer
RLC	Regulatory light chain
RPM	Revolutions per minute
S1	Subdomain 1
S2	Subdomain 2
SD	Standard deviation
ss	Single stranded
SVHS	Super VHS
TIFF	Tagged image file format
µL	Microliter
µM	Micromolar
V	Volume
V1	Volume 1
V2	Volume 2 as in C1 V1 = C2 V2
WLC	Worm-like chain model
XRD	X-ray diffraction

CHAPTER 1

INTRODUCTION

1.1 Clinical Basis for Structural Study

Inherited cardiomyopathy called hypertrophic cardiomyopathy (HCM) is an autosomal dominant disease that affects people of all ages. The most noticeable characteristic in HCM patients is the large number of young people (<35 years old) who experience sudden death. There are three subgroups of sufferers: those with high risk for sudden death, heart failure, or atrial fibrilation. In fact, with an incidence of 0.2% of the population, HCM is the world's most common inherited cardiovascular disease (Georgakopoulos and Tolis, 2007). Generally, a loss of function of sarcomeric proteins in cardiac muscle causes the heart to overcompensate and overexert itself. This compensation builds the walls of the left ventricle and causes the interventricular septum to become smaller. While somewhat similar to the thickening that occurs in the hearts of high performance athletes, a healthy "athlete's heart" tends to thicken symmetrically without a loss of function (Rawlins, Bhan et al., 2009). In contrast, HCM patients have an overly thickened left ventricle that cannot pump a normal volume of blood. Thus, their hearts are rendered less efficient. Over time, the thickening leads to abnormal pressures, which lead to stress in the ventricle walls, and to ischemia which kills heart cells and causes fibrosis in the heart (Maron, 2002). This pathogenesis can culminate in sudden death. While the disease is clearly genetic, factors like diet and exercise can also affect blood flow and can contribute to the outcome.

As of 2005, over 200 different mutations have been reported. This number is large and thus causes problems when genetic screening is attempted. For this reason, most diagnosis comes only after the patient presents with symptoms corresponding to their phenotypic subgroup. The

variety of mutations is largely due to intragene polymorphism. As a result of this diversity, even single missense amino acid changes in β cardiac myosin are implicated in this condition and can lead to sudden death (Debold, Schmitt et al., 2007). The onset of HCM may be caused by one of several mutations in myosin binding protein-C (MyBP-C), troponin-T, or in the myosin itself. This study focuses on mutations to myosin. One hypothesis is that mutations in the S2 region of myosin cause a loss of flexibility in the myosin that contributes to the malfunction and subsequent hypertrophy or thickening of the left ventricle of the heart (Cuda, Fananapazir et al., 1997).

The location of these problematic mutations is consistent with the functional regions of the contractile molecule. It has been reported that a substitution in β-cardiac myosin in the S1 at $403^{\text{arg-gln}}$ results in a phenotype that includes early onset, 100% penetrance in adults, and a high rate of the sudden death (Epstein, Cohn et al., 1992). This location is on the binding site for actin. It makes sense that a mutation that might affect binding to form the cross-bridge is implicated in pathogenesis. In relation to our study, a single mutation in the β-MHC gene on the C-terminal side of the S1/S2 hinge gives rise to abnormal actomyosin interaction as well. This mutation is characterized by 63% penetrance in adults and gives rise to sudden death less frequently than the S1 mutation. Clinical observation is corroborated by a single molecule in vitro motility assay that found a five-fold decrease in the rate of actin sliding by myosin with a missense mutation at $908^{\text{Lue-Val}}$ compared to wild-type (Cuda, Fananapazir et al., 1993). Also, in unpublished data from our lab, another lethal mutant at 930 has been shown to function differently than wild-type. However, this is just one of many mutations that lead to sudden death or HCM with less lethal outcomes. In fact, in the second leading cause of HCM, mutations to myosin binding protein C are thought to trigger haploinsufficiency of the MyBP-C (van Djik et

al., 2009). This effect is related because the binding site on the myosin for MyBP-C is very near the S1/S2 hinge. The MyBP-C is thought to act as a tether to the S1 and it's binding is not thought to affect the structure of S2 (Gruen and Gautel, 1999; Harris, Rostkova et al., 2004), however it is clear that a mutation (E924K) in S2 prevents MyBP-C's binding. Consequently, it is not unreasonable to infer that normal concentrations of the regulatory protein are needed to maintain S2's functional stability. The other mutations that affect myosin directly to cause HCM are also largely located in this same hinge region. There seems to be an issue with the onset of HCM and the loss of flexibility either directly by mutation to the cardiac myosin itself, or indirectly via the mutations to regulatory elements like MyBP-C. In any event, S2 and the hinges that border it play a role in normal muscle function probably by way of conferring flexibility to the molecule to deal with the forces brought on by the powerstroke. Consequently, S2 and its hinges are of much importance in this study and much of the discussion will involve S2's flexibility and stability.

1.2 Myosin Homology

There are over 20 classes of myosin. Some forms are similar and do analogous jobs, however, some have very different primary structures. Myosin heavy chain (MHC), is the main motile protein in nature, is found in nearly all eukaryotic cells. There are non-muscle myosins and muscle myosins. The myosin essential light chains (ELC) and regulatory light chains (RLC) and the heavy chain (MHC) are all part of myosin and all coded for by different genes. From an evolutionary perspective, it appears that the ELCs and RLCs, and MHC in smooth and striated muscles diverged even before invertebrates and vertebrates (Oota and Saitou, 1999). Non-muscle myosins are the furthest removed on the phylogenetic tree compared to the isoforms experimented on in this study. After that, the differences in smooth muscle and striated muscle

are less, although smooth muscle myosin is conserved in the region analogous to S2 in striated muscle. The striated muscle myosins can be found in invertebrates like the scallop. For many years, one of the best models for myosin in force studies was scallop muscle myosin. It was particularly useful because its X ray crystallography had been solved with high resolution. Scallop myosin shares about 40% identity with vertebrate skeletal myosin. Part of the problem solving these filamentous structures is the flexible nature of the S2 subfragment. To resolve the scallop structure, a leucine zipper was added near the S1/S2 hinge to confer stability to the coiled-coil region. As understanding has increased with better models, it is now possible to use vertebrate myosins that can be either skeletal or cardiac isoforms. The differences between vertebrate skeletal and cardiac myosins are few and their divergence is the most recent. Clinical investigations of HCM necessarily study human isoforms of the β cardiac myosin. The following force studies employing the GFS use rabbit skeletal myosin. The vertebrate skeletal myosin and human heart myosin shares some 75% identity in amino acid sequence and much of the gaps that are not identical are conserved, meaning that the difference from one isoform to the next might trade one hydrophobic residue for another or one charged residue for another of the same charge. Thus, the function is conserved even across species. When comparing the S2 between rabbit and human isoforms, 78% identity is reached with no gaps as seen in Figure 1. This makes the effective identity even greater than 75%, and positions rabbit skeletal myosin an excellent model for human cardiac myosin.

```
Score = 40.8 bits (94),  Expect = 5e-09, Method: Compositional matrix adjust.

Identities = 32/91 (35%), Positives = 53/91 (58%), Gaps = 8/91 (8%)


   H   GSS-PLLKSAEREKEMASMKEEFTRLKEALEKSEARRKELEEKMVSLLQEKNDLQLQVQA  59
       GS  PLL  A +E+EM    ++  ++KE L K+E  +KELEE+ V+LL++KNDL
   S   GSHMPLLSIARQEEEMKEQLKQMDKMKEDLAKTERIKKELEEQNVTLLEQKNDL------  54

   H   EQDNLADAEERCDQLIKNKIQLEAKVKEMNK  90
          ++   E++ ++L+     LE +V  + K
   S   -FGSMKQLEDKVEELLSKNYHLENEVARLKK  84
```

```
Score =  168 bits (426),  Expect = 3e-46, Method: Compositional matrix
adjust.
Identities = 99/126 (78%), Positives = 113/126 (89%), Gaps = 0/126 (0%)


 H    PLLKSAEREKEMASMKEEFTRLKEALEKSEARRKELEEKMVSLLQEKNDLQLQVQAEQDN  63
      PLLKSAE EKEMA+MKE+F R KE L +SEARRKELEEKMV+LLQEKNDLQLQVQ+E +N
 R    PLLKSAEAEKEMATMKEDFERAKEELARSEARRKELEEKMVTLLQEKNDLQLQVQSETEN  901

 H    LADAEERCDQLIKNKIQLEAKVKEMNKRLEDEEEMNAELTAKKRKLEDECSELKRDIDDL  123
      L DAEERC+ LIK+KIQLEAKVKE+N+RLE+EEEMN++L AKKR LED+C  LKRDIDDL
 R    LMDAEERCEGLIKSKIQLEAKVKELNERLEEEEEMNSDLVAKKRTLEDKCCSLKRDIDDL  961

 H    ELTLAK  129
      ELTL K
 R    ELTLTK  967
```

FIGURE 1 Myosin S2 sequence alignment between species. The first alignment is between human β-cardiac myosin and scallop muscle myosin (H=human, S=scallop), and the second is between human β-cardiac myosin and rabbit skeletal myosin (H=human, R=rabbit).

1.3 S2 Structure

The S1 head and S2 make up the heavy meromyosin (HMM) and C-terminal end of the S2 domain links to the light meromyosin or LMM, which make up the bulk of the fibrous portion of the protein. The S2 is an alpha-helical domain. Myosin II and Beta Cardiac myosin (in fact, most classes of myosin) exist as a dimer, so this S2 region forms a native coiled-coil by virtue of the hydrophobic residues following the slightly skewed heptad repeating unit. Subunits forming the heptad are *a-b-c-d-e-f-g* where *a* and *d* residues are hydrophobic and form the internal structure of the coiled-coil. The other residues are on the outside of the coiled-coil and can interact with each other or other residues in proximity to affect stability. The junction between the S1 and S2 is characterized as a hinge or a less stable region that tends to behave like a random coil than a more stable coiled-coil or naked alpha helix. Furthermore, this is an area that is suspected to contribute to myosin's flexibility as it pertains to its role in the powerstroke according to the sliding filament model. The hinges themselves might contain all of the necessary elasticity to fulfill S2's role, or this flexibility might spring from the random coiling and uncoiling along the length of the dimer at the S2 region starting at the S1/S2 hinge. This might not be dissimilar from events in the processive motors of non-muscle myosin VI where larger-than-expected step sizes are accounted for by the unstable melting of the dimer at the domain analogous to S2 (Rock, Rice et al., 2001). This observed melting along the domain analogous to S2 presumably starts at the already less-stable hinge region. Proteolytic digestion of the myosin dimer leaves monomeric S1 capable of producing a powerstroke and moving actin along in a single molecule assay (Toyoshima, Kron et al., 1990). It is clear that S2 is not needed for S1 to undergo powerstroke, however, it is noted that the force generated in the cleaved S1 is less than that measured with the native protein. Different isoforms of β cardiac myosin exhibit

the same amount of force generation (Sugiura, Kobayakawa et al., 1996). Perhaps the difference lies in the role of S2. There remains room in the sliding filament model for S2's flexibility to contribute to powerstroke function and force generation. Myosin's flexibility was also demonstrated in an in vitro motility assay when it was observed that the myosin can move actin in a bi-directional fashion (Toyoshima, 1991). Also, the question of the nature of S2's elastic properties remains, as experimental observations are not precise enough to divine whether this is primarily a function of random coiling in the hinge regions, a function of dimeric melting along the length of S2, neither, or some of both.

1.4 Flexibility of the Rod

What is the nature of this proposed flexibility? There have been many interesting observations to contribute to the debate on this topic. One way of framing the role of S2 and its hinges is that the flexibility is a way to dampen or reduce shock from the cycling force loads of powerstroke. As the force is transmitted from the S1 along the HMM, the hinge region/s could be thought to absorb some of the force to protect the structure of the LMM which is necessary to keep the thick filament intact. The coiled-coil of S2 is made up of relatively rigid α helices. The hinges are comparatively less rigid and could flex as force is transmitted parallel to the rod. In fact, the observed distance of S1 displacement during conformational change is approximately the same (10 nm) as the amount of stretching out the S2/LMM hinge undergoes in AFM experiments using approximately 40 pN of force (Root, Yadavalli et al., 2006). So, it would be reasonable to expect to see lengthening up to 10 nm upon applying graded resistance to S2 if the nature of S2's flexibility is mostly due to the relative instability of the hinge regions.

Another way to think of S2's flexibility is in its role forming the actomyosin crossbridge. S1 needs minimum degrees of freedom to attach to F-actin. Because myosin II is dimeric, there

are two heads per molecule and one or both can form crossbridges with actin. Resonance energy transfer (RET) indicates the location of S1 binding on actin is highly dependent on steric hindrances levied by the regulatory troponin complex. Also, these structural studies show that S1 must bind in a pre-powerstroke conformation (Castro-Zena 2007). Best-fit docking modeling indicates that S1 might need to tilt over 30^{o} upon attachment to the thin filament. The entire series of conformational changes includes neck-region movement, and tilting of the catalytic domain with associated twisting. This produces an interaction distance of up to 19 nm (Root, Stewart et al., 2002). Twirling was observed in a gliding filament assay where whole myosin II rotated actin with as much as a micron of pitch (Beausang, Schroeder et al., 2008). This is consistent with the observation of the tilting of the catalytic domain on a single molecular scale. To function in these parameters, there has to be some mechanism of flexibility in the rod. It is thought that the dimer might uncoil starting at the S1/S2 hinge. S2 might uncoil or melt to allow S1 the degrees of freedom to attach to actin. In this case there is torque applied to the dimer as opposed to force transmitted parallel to the rod. In this view, as the dimer melts, the separated α helices revert to a random coil, which is less rigid, less stable, and more flexible. Because of the nature of the repeating hydrophobic residues that facilitate super coiling, it is reasonable to think that the more uncoiling S2 goes through, the less stable the dimer becomes and the more the molecule will lengthen under load to preserve the other structures.

Still, another way to think about this process is to reintroduce parts of some of the first models regarding muscle contraction. Before electron micrographs (Nachmias and Huxley, 1970), before the sliding filament model (Huxley and Simmons, 1971), even before the observance of striation in muscle fiber, there was a less sophisticated view of muscle contraction. Simply, the model supposed that muscles worked much like a rubber band. The key is the elastic

property that could extend under force and snap back into place generating force. In light of the mountainous evidence that supports the sliding filament model, and the observation of isometric muscle contraction, which refutes a rubber band theory, there is no paradigm shift proposed here. However, it could be useful to revisit the idea in the context of S2 and its hinges. While muscle contraction is indeed accomplished by the relative sliding of the thick and thin filaments, there remains a role for elasticity to fully complete the nuances of the sliding filament model. It is not unreasonable to imagine and even test the instability of the hinge, which is just a region of the rod that does not conform to the stable and rigid coiled-coil. If the hinge is unstable, conforming to random coil, then it follows that there is a certain amount of variable displacement the hinge can accomplish under load. Also, if the dimer undergoes uncoiling under load and rewinding by entropic effects, the end result would be similar to the elasticity of a rubber band.

1.5 Atomic Force Microscopy

Force studies are common in physiology. As the scale of the assay decreases, methods become less reliable when determining force for single molecules at physiological levels (these are on the order of piconewtons). Atomic force microscopy (AFM) has a proven track record of resolving lengths of biological samples with distance measurements on par with many electron microscopes. Additionally, AFM is able to determine forces applied to the samples by virtue of their cantilever arms, and their tips, which contact the specimen. These cantilever arms must be carefully calibrated and by their nature, calibration between different AFM instruments or even between assays is unreliable (Sattin, Pelling et al., 2004). Each cantilever arm has a spring constant which is initially unknown. This problem is compounded when different buffer solutions, different tips, or different surfaces are used. The resolving power in relation to force measurements (tens of piconewtons) is often below that required for single molecules such as

myosin. Binding specificity to target regions of proteins is a time consuming prospect. Tips that employ an antibody for sample attachment can often only be used once. Tips that rely on less specific hydrophobic interactions can be put through many paces, but there is always the question of where the binding is taking place potentially convoluting the measured length of the molecule. AFM is capable of providing splendid pictures with resolutions rivaling electron microscopy, however, when using tips designed for imaging, there is no force data by virtue of the patterns the tip follows to interact with the surface. Previous work has proven valuable in describing the action of the powerstroke with an AFM. It has been shown that there are three discrete stages in the actomyosin crossbridge: the rise (R), extension (E) and plateau (P) phases (Root, Yadavalli et al., 2006). These phases show the structural nature of the subfragments of the protein by virtue of how much force it takes to unravel the characteristically different parts. In this study, AFM experiments suggest that S2's flexibility is necessary for complete R whereas LMM alone gives the shortest length of R. In other words, a longer R correlates to more flexibility, and in the assay, the fragments with S2 always had significantly longer R at very low force than LMM alone. Also, where the rod is intact and its hinges present, length of R increases. This supports the idea that not only the coiled-coil, but also the hinges on either terminus contribute to the molecule's flexibility in a characteristic way not seen in other globular proteins. The AFM is well suited for such an experiment as it can deliver the necessary forces to cause the entire molecule to stretch out before it detaches from the cantilever around 200 pN.

Force studies are not limited to proteins. The AFM has successfully been used to determine that stacking interactions of DNA are more important than hydrogen bonding in relation to the stability of the double helix (Sattin, Pelling et al., 2004). In other words, longer ds DNA requires more force to shear the double helix than in shorter segments. The AFM system

was refined to acquire force resolutions on the order of 10-20 pN. This research also uses a clever approach of coupling oligonucleotide microarrays with the force data in order to ensure that perfectly matched short oligonucleotides could be directly compared in different runs. This study is also pertinent because the data is compared to our own data using 12 base pair oligonucleotides. We measured similar results with our system. DNA was chosen because the lengths are already known and because the double helix is analogous to the coiled-coil region of S2.

1.6 Optical Traps

Optical traps (OT) have been used to describe the S1/S2 hinge area as well as other biological samples. It has been shown that myosins with leucine zippers inserted near the hinge lose contractile function as compared to those with zippers incorporated further down the molecule towards the C-terminus (Lauzon, Fagnant et al., 2001). Furthermore, this study suggests that the step size in dimeric myosin II is double that of the monomer, and that the motion of the two heads is probably coordinated for optimal performance. This study supports the idea that the coiled-coil dimer is capable of unwinding and rewinding. In another study, evidence shows that double headed myosin produces twice the displacement and force as single headed myosin (Tyska, Dupuis et al., 1999). In other words, double-headed myosin attached to actin can displace the actin by about 10 nm at a reported force of about 1.4 pN whereas single headed myosin translates actin 6 nm at 0.7 pN. A different OT study measured the similar displacement but with a force of 3.3 pN (Miyata, Yoshikawa et al., 1995). In either event, the force levels for a single powerstroke are too low to currently be resolved by AFM. The resolving power of OT is on the order of sub-piconewtons to hundreds of piconewtons for force measurements and can track displacements in nanometers. However, measuring the absolute

length of the molecule is less accurate than AFM and on par with GFS. The system is also excellent for resolving temporal measurements. The main advantage of OT to the proposed GFS is the force can be changed in real time, whereas the force in the GFS is determined upon analysis of the data set and cannot be changed on the fly. OT uses the momentum of light and positions beams to hold microspheres in space. These beads can range in size up to about 50 microns in diameter. Their precision is impressive; however, there are a few issues that are inherent in the system that could be addressed by considering using GFS. Each OT must be calibrated regularly according to the bead size and the power of the laser. Again, there is no issue with calibration on a GFS because of the constancy of Earth's gravity and the known density of glass. To suspend large beads and manipulate them in space to cause a force load on the sample, the lasers must be proportionally powerful. If cost were no option, there is still a problem in that a high-powered laser focusing very close to a biological sample tends to do two things. One, it will heat up the sample. Because thermodynamic stability is a key issue with protein denaturation, this variable is not trivial. This is especially relevant if the measurement is to be carried out at equilibrium like the ones using GFS. Also, it has been shown that the laser contributes to photodamage of biological samples due to irradiation. Different wavelengths of light do different damage to different samples. So care must be taken when choosing a light source that might work for one type of biological sample, but be damaging to others (Nabiev, Ovsiannikov et al., 2008; Zhang and Liu, 2008). Finally, the use of light to suspend beads with a tethered molecule limits the potential use of fluors because the wavelength of light can photobleach probes. With GFS, probes can be incorporated easily. This is not to undermine the role of OT, but to give another, less expensive option when the constraints of the OT system have been considered.

1.7 Computer Modeling

Computer models can determine the relationship between force and distance by combining solved crystallographic structures with algorithms that control for temperature, pH, time, and other factors. In unpublished computer simulation data from the Root lab, wild type human β-cardiac myosin is stretched with a force of 16 pN parallel to the myosin rod compared to myosin with single a deletion at AA 930. Results show that even a single point mutation in a sensitive location contributes to instability in S2 coiled-coil according to the model. Also, in a recent computer simulation at non-equilibrium, there is some evidence that suggests there is more lateral flexibility than along the length of S2 using a scallop XRD model (Adamovic, Mijailovich et al., 2008). This is the type of structural evidence that the GFS can support or disagree with by comparing force spectra. There are some significant differences, however. The main difference is that the GFS is designed to stretch at equilibrium, and while that is not theoretically problematic for the computer simulations, it causes practical problems because it takes very long amounts of time to do the simulations slowly. Thus, modeling is often done with much higher force loads at very short (picoseconds) time intervals.

1.8 In vitro Motility Assays

Work on single molecules became more viable with the development of the gliding filament assay. In this set-up, myosin fragments are attached to glass slides and actin is introduced in the presence of Ca^{2+}, or ATP, or ADP, or other reagents depending on what was being studied. The fluorescently labeled actin is then monitored and it's speed and direction are noted. The faster a filament of actin is translated, the more efficient the motor protein is depending on the variable under study. This work is important because it gives direct structural evidence describing what the motor proteins are capable of by themselves. For instance, it was

shown that single headed S1 can move actin by itself and that S1 with S2 moves actin at a higher rate than S1 alone (Toyoshima, Kron et al., 1987). Also, myosin is capable of translating actin in a bidirectional fashion indicating that actin has an innate polarity that determines which way it is to travel (Toyoshima, 1991). These types of set-ups allow aspects of in vitro motility assays to be combined with OT assays where the slide with attached motor proteins can be brought near the tethered molecule in an OT so the proteins can interact (Rock, Rief et al., 2000). This way, force can be measured in vitro. While these methods show evidence of myosin's flexibility (Toyoshima, 1991; Lauzon, Fagnant et al., 2001), direct structural evidence has not been presented that reveals the nature of the rod's flexibility.

1.9 Introduction to the Gravitational Force Spectrometer

A novel instrument used for force and distance measurements is the gravitational force spectrometer (GFS). Developing the GFS to make accurate and precise measurements is at the heart of my work. Generally, this instrument incorporates a light microscope fitted with a video or digital video camera. The scope is mounted on an equatorial mount that allows the scope to be rotated around two different axes for almost unlimited degrees of freedom. On a standard microscope slide are attached glass microspheres that have tethered to them the molecule of interest and a mobile bead on the opposite end. This makes a pair of beads via the sample's attachment to both. As the scope rotates, gravity acts on the mobile bead in certain orientations and distance measurements can be made from the centroid positions of the microspheres using the video system and NIH's ImageJ software. The distance of the tethered molecule can then be determined. This method of determining distance is very similar to the system employed with OT. This system benefits from the self-calibrating effect of living on planet earth. The gravity exerted on the mobile spheres can be calculated to hundredths of piconewtons because the

differences in gravity on the surface of the planet are negligible especially when these forces are acting on glass beads of relatively small masses and uniform density.

Because this is a novel instrument, much of the capabilities and applications of the GFS remain hidden. As it is now, the system can be divided into (a) mechanical components: including the microscope, its mount, and its base; (b) video component: the camera; and a (c) computer component: all the software to manipulate images and analyze data. There is also the bead preparation, which is a separate, preliminary laboratory protocol. Many improvements to the system have been made and they will be briefly discussed here. Mechanically, modifications to allow more degrees of freedom in space have been implemented. Using a functioning air table for the base of the GFS helps reduce noise. Permanently immobilizing the swiveling head of the microscope is useful for predicting the location in space of d_{max}. Different stage configurations have been considered and settled. The objective lenses have been of particular benefit when using the most appropriate one for different circumstances. While virtually all of the reported measurements employ the original analog camera, it is clear that moving to the newer digital video camera has several advantages. Because of this improvement, data storage moves from SVHS tapes to an external hard drive. New software and a newer computer facilitate the transition to an all-digital format nicely. Plug-ins in ImageJ have been refined and the thresholding technique has been greatly improved. On the analysis side, smoothing the data via a rolling average tends to fit better into the three-tiered formula that yields the final distance measurement. Analyzing beads independently in a pair together with careful threshold settings have reduced the error in the distance measurement by as much as four times. As the experiments progressed, simple improvements in lab technique have proven vital. Initially, the myosin tended to clump when added to the beads because it is necessary to agitate the mixture

for antibody attachment to the myosin. Moving from a vortex to a slow rotator, which tumbles a microcentrifuge tube once a minute eliminates this problem. Slight improvements to building the cell on the microscope slide prevent the sample from drying out by creating a tightly sealed chamber.

1.10 Experimental Design

The experimental design of this project is to apply force to the molecule and measure its distance or any stretching between attachment points of site-specific monoclonal antibodies. The MF20 antibody binds to a region on the LMM on the C-terminal side of the S2/LMM hinge. The MF30 antibody binds on S2 on the C-terminal side of the S1/S2 hinge. Figure 2 illustrate the possibilities for binding coated microspheres to myosin. My work can be divided into three main assays including a control using 12 bp DNA; force applied parallel to the myosin S2 coiled-coil; and force applied perpendicular to the myosin S2 coiled-coil. In the first assay, the glass microspheres are coated with terminal amines that can react with and bind to the ends of the DNA. This assay acts as a control because the results can be compared to previous work that tests forces applied to the double strand of DNA at different base pair lengths and finds a rupture force that increases as the length of the DNA increases. My results are comparable to the results from the Sattin lab using an AFM that describe a rupture force of about 20 pN for 12 bp ds DNA. The second experiment explores the role of S2's elasticity by stretching the rod from N-terminus to C-terminus. This is designed to see if the hinge regions increase in displacement with increased load. The results do not show this trend, but the error in this assay is more than the amount of expected stretching, so the hypothesis cannot be rejected. In the third assay, the S1/S2 hinge is pulled apart. This is also to explore the role flexibility plays in the region as force is

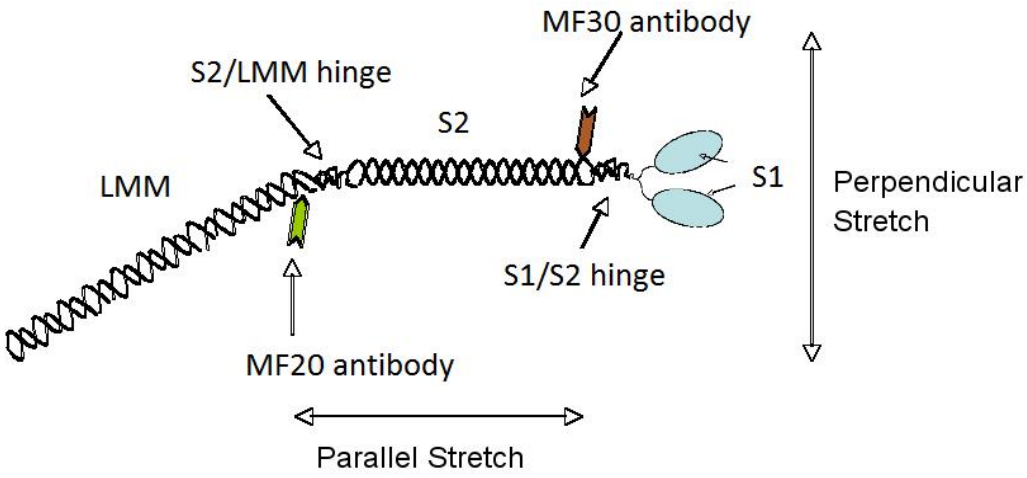

FIGURE 2 Schematic of myosin and antibody attachment sites. Microspheres tether rod by attaching to antibodies. The MF30 is near the S1/S2 hinge. The MF20 antibody is near the S2/LMM hinge. Applying force between these two antibodies will stretch the coiled coil parallel to its axis. Applying force between two MF30 antibodies attached to each of the two epitopes on the dimer near the S1/S2 hinge will stretch the coiled coil perpendicular to its axis.

applied perpendicular to the rod. The results are consistent with the idea that the coiled-coil unwinds in response to force and that this activity does allow the S1 domain more freedom when binding to actin. In all three assays, the GFS undergoes transformation and refinement. By the third assay, the error in displacement measurement is reduced to a reliable level. Many more improvements can be made, and this points to a useful future for the GFS.

1.11 Hypotheses

This work is based on the idea that S2 and or its hinges allow for flexibility during the powerstroke. This is supported by many cited observations. If true, this flexibility should be able to be measured at forces low enough to be in the physiological range as applied to a single molecule. This study has two main points of emphasis. One is the development of the GFS as a new contributor to the field of structural biochemistry. The other area of emphasis is on the biological implications involved in the proposed flexibility inherent in the myosin molecule.

Novel Instrument, Hypothesis 1: the GFS is sensitive enough to measure the absolute lengths of 12 bp DNA and the myosin molecule. The GFS can accurately measure forces imparted by small glass microspheres on a tethered molecule. The GFS can measure any stretching occurring at a physiologically relevant force range on myosin, and the system can measure stretching as force is applied parallel to the rod or perpendicular to the rod.

Biological Relevance, Hypothesis 2: Imparting force to the S2/LMM hinge should stretch it out by as much as 10 nm. This confirms the idea that the hinge is indeed flexible and capable of absorbing the forces from muscle contraction and the displacement brought on by conformational change from a single powerstroke event. Imparting force perpendicular to the rod should pull apart the dimer. This confirms that S2 can undergo melting to allow more

degrees of freedom for the binding of S1 to actin and shows that the S1/S2 hinge does indeed uncoil as a part of its normal function as has been observed in non-muscle myosin VI.

CHAPTER 2

MATERIALS AND METHODS

2.1 Bead Preparation

To measure biomolecules, the gravitational force spectrometer (GFS) relies on attaching the molecules to glass beads. These glass microspheres range in two sizes from 3-10 microns and from 10-30 microns in diameter. Glass beads are chosen for their properties. Because they are made of glass, their densities are all the same at 2.5 g/cm^3. Thus, their measured volume gives the amount of gravitational force the mobile bead imparts on the molecule by the following equation: $F = V(d\text{-}b)\,a$ (F = force, V = volume, d = density of the glass, a = acceleration due to gravity, b = the density of the displaced water). This range of beads is capable of imparting forces from 0.2 to 208 pN. Another characteristic of glass microspheres is their ability to focus light through their centers. This makes centroid analysis with a video system viable. Round glass beads also do not tend to aggregate. However, during the course of this study, it is worth noting that many glass beads appear to be fused to one another as part of their manufacturing process. This can lead to measuring erroneous pairings; however, these are culled out upon analysis. It is possible to color label the beads from different batches so that apparent pairings can be ruled out if they are the same color. At present, this does require the use of fluorescence microscopy in addition to the GFS apparatus. Several unsuccessful attempts were made at trying to fractionate the beads by size or anomaly by pumping them through viscous glycerin, but they tended to clump together and pass through microtubing as one unit.

The process for coupling terminal amine groups to the beads is crucial for attaching subsequent antibodies or nucleotides. The process is adapted from Weston and Avrameas (Weston and Avrameas, 1971). Adding the terminal amine groups is a simple process of

submerging the glass microspheres in 0.04% 3-aminopropyltriethoxysilane in acetone for two minutes. Glutaraldehyde is cut with acetone to obtain a 5% glutaraldehyde solution. The aminosalinated beads are shaken in the glutaraldehyde solution and rotated for three hours at room temperature. After centrifugation, the supernatent is discarded and a coupling buffer is added to the cake of beads.

For the experimental group, the monoclonal antibodies are added in a coupling reaction with the glutaraldehyde treated beads. Specifically, the MF30 antibody is raised against the S1/S2 junction and the MF20 antibody corresponds to the S2/LMM hinge region. These antibodies are raised against rabbit skeletal myosin II. For the control group, the 12 bp DNA is added without any antibodies because they are added as single stranded DNA that can react with the terminal amine groups on the beads. Either mixture is incubated for 24 hours. Upon centrifugation, the supernatant is discarded and a glycine quenching solution is added for 30 minutes with agitation to quench the unreacted glutaraldehyde. The beads are then washed several times and stored in low salt buffer. For the DNA control group, the beads are ready to be used. For the experimental group, the myosin is added near the time of the experiment. In the myosin experimental group, the beads are stored with the antibodies until the experiment is ready.

Before adding the myosin to the antibody-coupled beads, the concentration of the stored myosin must be cut from 160 μM to 5 μM. This is done by adding high salt buffer according to the formula $C_1V_1 = C_2V_2$ where the final volume is 400 μL (the final volume accounts for the volume of myosin, buffer, and beads). When the right concentration of myosin is obtained, a few microliters of beads from two separate bead preps can be added and slowly rotated for two hours. For instance, in an experiment where force is applied parallel to the coiled-coil, there

must be a stock of beads prepared with the MF20 antibody and a different one containing the MF30 antibody. These monoclonal antibodies were raised against sequences of rabbit skeletal myosin. It has been shown in rats that the MF20 antibody binds with specificity on the LMM on the C-terminal side of the S2/LMM hinge (Shimizu, Dennis et al., 1985). The MF30 binds on the C-terminal side of the S1/S2 hinge. This selects for a bead attachment near the head region and a different bead to attach near the LMM. If the size of the beads is the same, then a 1:1 ratio of beads is added to the 5 μM myosin. However, in some of the runs, big beads were paired with small beads. For those mixtures, a 9:1 ratio of big beads to small beads works better. Care must be taken not to over-stimulate the beads in the myosin and buffer, for the myosin tends to clump up if subjected to vortexing even at low power, however, it is necessary to agitate the beads to encourage pairing. To avoid clumping, beads mixtures with myosin can be rotated in microcentrifuge tubes slowly, or hand tumbled. The best way was to tape the top of the microcentrifuge tube to the center of the second hand of a wall clock and let the prepped beads spin around at one RPM for 30 minutes.

2.2 Sealed Flow Chamber

Before measurements can be made, a specialized chamber not dissimilar from a flow cell adapted from in vitro motility assays and modified with nitrocellulose (Toyoshima, Kron et al., 1987) must be constructed to provide a sealed environment that can be rotated in space. A standard microscope slide is submerged in 0.1% nitrocellulose providing the glue needed to anchor the larger beads of a bead pair (a pair of beads attached by a molecule of myosin between attached antibodies) to the glass slide. After the nitrocellulose has dried, a chamber is constructed on the face of the slide by cutting strips of glass and arranging them in a box to contain the sample. A bead of vacuum grease anchors these strips of glass to the base slide.

Once the box is complete, the experimental beads can be pipetted onto the surface of the base slide. The required volume of beads is only 2-4 μL, so it is important to tap the pipette tip on the glass without pressure over the area of the chamber, and then slowly release the rest of the contents of the micropipetter. This avoids clumping all the beads into one area on the slide in an effort to get a reasonable distribution on the surface. After the beads are on the surface of the slide, 200 μL of high salt buffer are added to the chamber and a coverslip is attached with vacuum grease to close the cell. The high salt buffer is used to prevent the LMM of the myosin from forming long filaments through higher ordered symmetrical hydrophobic interactions. For the DNA control, the low salt buffer is used. At this point all the beads are contained in a sealed buffer environment and are ready to be viewed by the GFS.

2.3 GFS Design

The heart of the GFS is a standard brightfield microscope equipped with three objective lenses that are used for different circumstances. When the prepared slide is staged, a Zeiss 25X (numerical aperture = 0.60) objective lens is primarily used for scanning the slide to find potential bead pairings to be measured. Once a suitable pair is found, usually the objective is switched to a 20X Zeiss lens with a significantly lower numerical aperture (NA) of 0.25. With the lowered NA, the resolution is also less than the other lenses, but the depth of field is increased. This is useful when a large bead is paired with a smaller bead. Because of size differences, the smaller floating bead might not be in focus at the same time as the larger anchored bead while using a high NA lens, the lower resolution and greater depth of field allow both beads to be imaged simultaneously which is crucial for centroid analysis of the archived movie. The 40X lens (NA = 0.65) is only used when one or both of the beads are so small that

they need more magnification, or require more gathered light to be measured with the current system.

Once a potential bead pair is identified, the GFS must be oriented in a way so as to go through a range of motion that has the floating bead pointing at the ground at its maximum distance from the anchored bead. A useful way to visualize the GFS in such an orientation is to observe the bead pair on the video screen. The smaller floating bead will be in one of four quadrants in relation to the big bead. For instance the video image in Figure 3 shows the floating bead stuck to the left side of the anchored bead, so the GFS should be laid over on its left side. This allows the small bead to float and gravity acts on the smaller bead. Also, the smaller bead is on the bottom half of the large bead, so after the GFS is laid over on its right side; the measurements can be made in 2.5^{o} increments where the base of the microscope arches toward the floor. The goal is to put a bead pair through a range of motion and take individual movies of the pair in 2.5^{0} increments. Each angle is recorded to SVHS videotape, or digital video to hard drive for later processing. It is worth noting that the image on the video monitor should not look different from movie to movie (angle to angle) of the same bead pair because the orientation of the camera follows the pair through space. In fact, it is important that the focus is held constant so the last movie looks just like the first movie. Initially, the most important part of the video capture is to keep the focus consistent and the GFS motionless during acquisition. The GFS is mounted on an air table to minimize vibrations during video capture. These vibrations are potentially problematic when recording a distribution of distance measurements whereby each 16.7 ms frame of video is measured and recorded. The majority of the data used is from an analogue video camera that shoots 60 frames per second. A typical movie is shot for 10 seconds

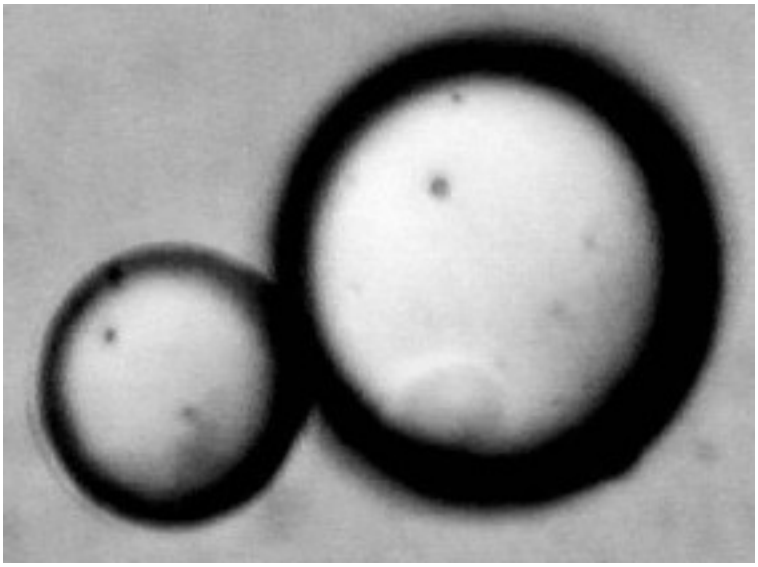

FIGURE 3 Image of a bead pair. This is an example of a single frame of video taken from experiment 2. The smaller glass microsphere is tethered to the larger bead by a single myosin and is allowed to move freely in the buffered chamber. Note: each subsequent movie should appear just as this one. The camera's orientation follows the beads through space retaining its initial position perpendicular to the axis running through the center of the pair.

FIGURE 4 Binary image of bead pair. This is an example of an early bead pair from experiment 1. Note: subsequent refinement of the thresholding process warrants separating and thresholding each bead independently.

yielding 600 frames of video. The raw video is stored on SVHS tapes. For processing, the video from the tape is captured using a video grabber installed on a Power Macintosh. Once the video has been grabbed, it can be manipulated in the digital domain with ImageJ software. This is emphasized at the grabber stage where the black levels are adjusted and optimized. Once this is complete, the video is moved to a PC with an Iomega zip drive. At the PC, the ImageJ is used to de-interlace the video so all the odd-lined video is in one clip and all the even-lined video is on another. After the movie is copied and the original is de-interlaced—even, and the copy is de-interlaced—odd via ImageJ plug-ins of the same name, the two movies are ready for thresholding. Better results were evident when the bead pair was separated and the big and small beads were thresholded independently. Under this independent bead thresholding, four movies are necessary: (a) de-interlaced odd big bead, (b) de-interlaced odd small bead, (c) de-interlaced even big bead, and (d) de-interlaced even small bead. Thresholding is the process by which each pixel in the movie is assigned a one or a zero. Once the movie is in binary form, a digital black and white image emerges. This is performed to give the interior line of the bead a more clean edge so the volumes can be calculated more accurately and so centroid analysis can be utilized. Centroid analysis is again performed in ImageJ. The concept is to take the centroid of each bead. The centroid is defined by its X and Y coordinates in space. Each frame of video measures the centroid position of each bead. Over the course of a 600-frame movie, the results for each frame are binned so that there are approximately 30-60 bins, and a distribution is compiled and solved to give a final distance measurement between the centroids of the paired beads. Figure 4 shows the distribution of one distance measurement for one angle of measurement, which corresponds to 600 frames of video. The measurements are binned and put into a solver formula in Excel, which results in the overlapped curve showing the relationship between the expected lowest

energy distribution and observed data to get a representative single distance measurement for that particular angle from the capture.

Over the course of an entire measurement where approximately 25 movies are made for a single bead pair, another pattern emerges. This is the distribution from the minimum (d_{min}) distance between centroids and the maximum (d_{max}) distance between centroids. A typical plot of distance measurements per each angle is shown in Figure 5. This ideally follows a normal two-tailed distribution where there is a d_{min} 12.5^{o} away from either side of the single d_{max}. However, skewed distributions can still be used and they indicate the floating bead is significantly off the equatorial axis of the anchored bead. At d_{max} of a sample whose floating bead is attached at the equator (angle β), the radii of the beads can be subtracted out and the result is the length of the tethered molecule. However, most pairings do not fall under these ideal criteria, and even if they did, there is no good way to know that by the microscope image alone. To deal with this, a strategy to fit the data is necessary. The microscope is tilted so that the objective lens is perpendicular to the force of gravity. Then, the microscope is rotated around the axis parallel to the objective lens (angle α) and the distance between centroids (d) of the mobile (radius = r_a) and anchored (radius = r_b) beads is recorded and plotted versus α to determine d_{max} (defining $\alpha = 0^{o}$) and d_{min}. If $\beta = 90^{o}$, then the length between antibody attachments (cord length = c) is simply $c = d_{max} - d_{min}$. However, since β is unknown, the geometry is more complex.

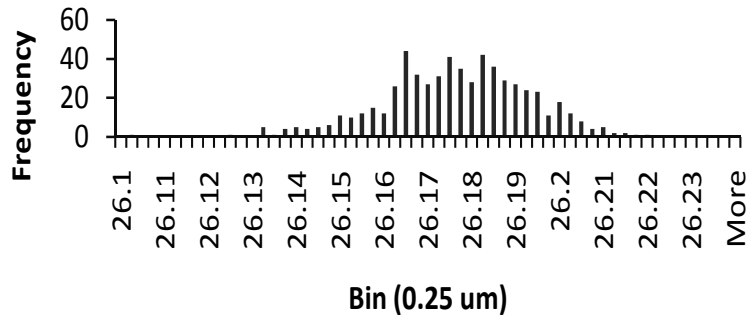

A

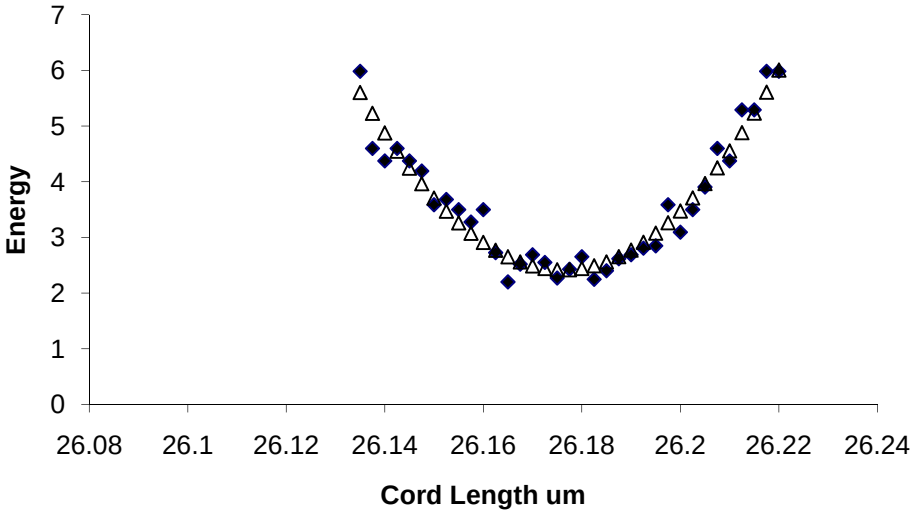

B

FIGURE 5 Centroid distance distribution. This is an example of distance data from one 600-frame movie where (*A*) is the normal distribution of binned centroid measurements for each frame of video, and (*B*) is the same data fitted against the *a priori* model that shows the distribution of distance measurements around the lowest energy. Diamonds are experimental data points and triangles represent expected outcomes. Good agreement leads to precise plotting of d_{min} and d_{max}. The distance is measured in microns.

However, both β and *c* can be determined by simultaneous fitting of the plotted data for α values less than or equal in magnitude to α_{min} (the value of α at first contact when $d = d_{min}$) to the following nested equation set:

$$d = [(g \sin \alpha)^2 + (g \cos \alpha + d_{max} - g)^2]^{0.5}$$

$$g = [d_{min}^2 + r_b^2 - (r_a + r_b)^2]^{0.5} = r_b \sin \beta$$

$$c = d_{max} - r_a - g$$

Fitting the data with these equations yields both c, and a high precision value for r_a that is used to calculate the microsphere volume and its force by the following equation:

$$F = V(d\text{-}b)\, a$$

Figure 6 shows a schematic representation of the above a bead pair configuration to visualize the formulas. Figure 7 shows the plot data that used to calculate the final displacement of the length of the molecule. The centroid data from ImageJ is dumped into Microsoft Excel for data analysis where the mentioned formulas are applied for a final distance measurement.

The video system is also useful for determining the radius of the floating bead very precisely. Originally, the user manually directs straight lines to bisect each bead, and the distance between pixel peaks on the drawn lines are averaged to give the radius. Improving on this, the image of the bead is manipulated to find the edges. Then, the image is thresholded to thin the edge. The spatial information for each emerging pixel can be solved for to find the radius of the bead based on the pixels/um^2 depending on the magnification of the lens. This is used to determine the amount of force the floating bead can exert on the molecule. The process is described in pictures in Figure 9.

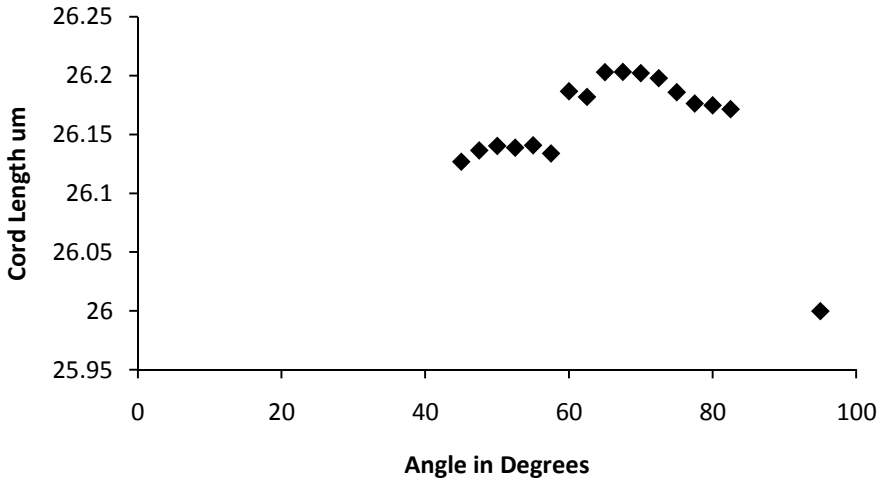

FIGURE 6 Plot of all angles for myosin 89. Each point represents all data from distributions seen in Figure 3. D_{min} is at 50°. α_{min} is estimated at 12.5° away from d_{max} in this set.

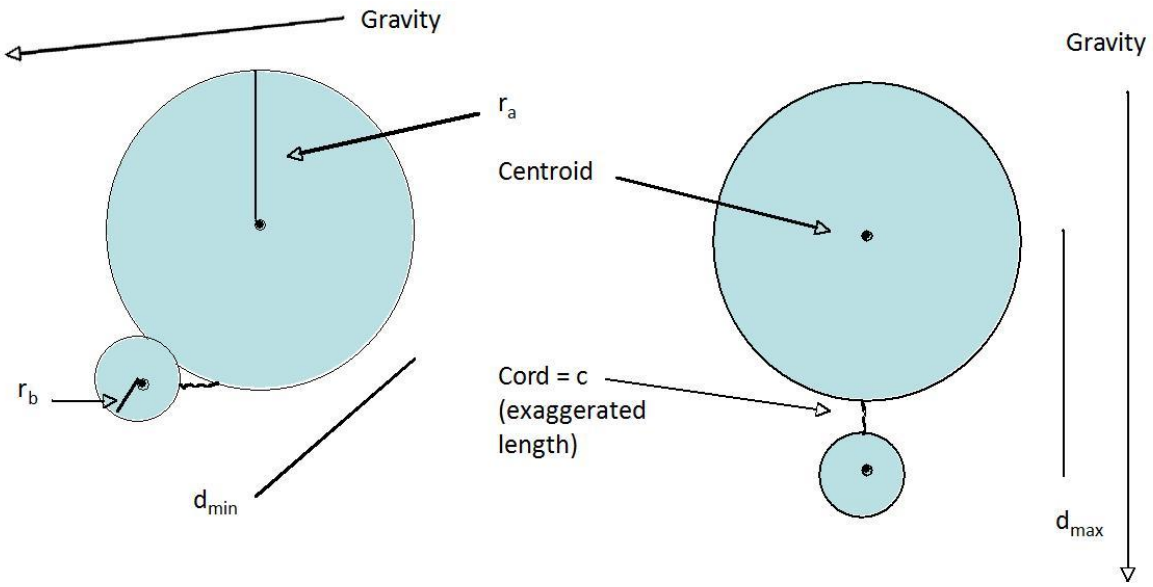

FIGURE 7 Schematic illustration of gravitational force spectrometer principle in 2 dimensions. Equations for fitting take 3-dimensional information into account as described in the original proposal. The different directions of gravity are indicated for the left and right panels. Gravity affects the relative positions of the large immobilized microsphere and the small mobile microsphere. The radii of the immobilized and mobile microspheres are r_a and r_b, respectively. Note that the distance between centroids, d, is at a minimum in the left panel and reaches its maximum in the right panel when the centroids and the molecule are in a line parallel to the force of gravity.

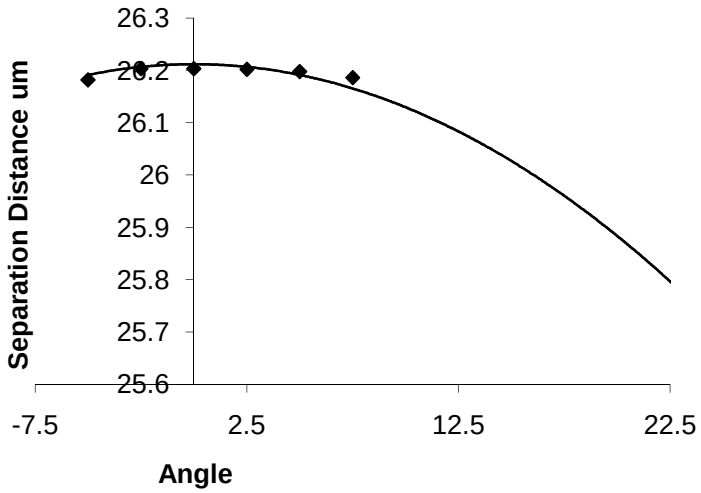

FIGURE 8 Fitted analysis of key measurements. This graph plots the key points between both d_{mins} from the distance graph from Figure 4. Note: d_{max} is at 0^{o}.

In the final analysis, both a force imparted by the mobile bead, and the cord length are calculated. The few samples that utilized the newer digital camera do not as need much processing as the analog movies. The digital movies are fed directly to the Intel Duocore 2 via Unibrain's FireI software where they are monitored and lossless compression is applied. They are then converted to TIFF files with VirtualDub software. They can then be imported to ImageJ from the external hard drive and thresholded and analyzed. This is when Excel takes over and analyzes and plots the data with customized spreadsheet functions developed in our lab.

2.4 Control Using 12 bp DNA

This series of experiments is divided into three specific protocols. The first is based on earlier work using an AFM and DNA of various bp lengths. Because the AFM experiments were able to give reliable experimental data concerning both the lengths of DNA and the rupture forces that sheer double stranded DNA, this is a good starting point for the GFS. Using 12 bp single stranded DNA, beads were prepared using the aforementioned protocol. Two separate bead preps with complimentary ss DNA are combined so that the complimentary strands anneal resulting in bead pairing with ds DNA tethered between a larger bead and a smaller bead. Note that the attachment is always with one bead on one strand and another bead on the other strand, never two beads on the same single strand for DNA. There is the possibility of multiple tethering per pair, however, their characteristics do not fit well in the equations and are thus thrown out. Two to four microliters are pipetted from the cake of beads at the bottom of the microcentrifuge tube onto the slide with an open chamber. 200 μL of low salt buffer is added to the open chamber to create the aqueous environment where floating beads can move freely in space. The final coverslip is added and the sample is ready for viewing. Upon adhesion to a nitrocellulose covered microscope slide, the larger bead anchors itself and the

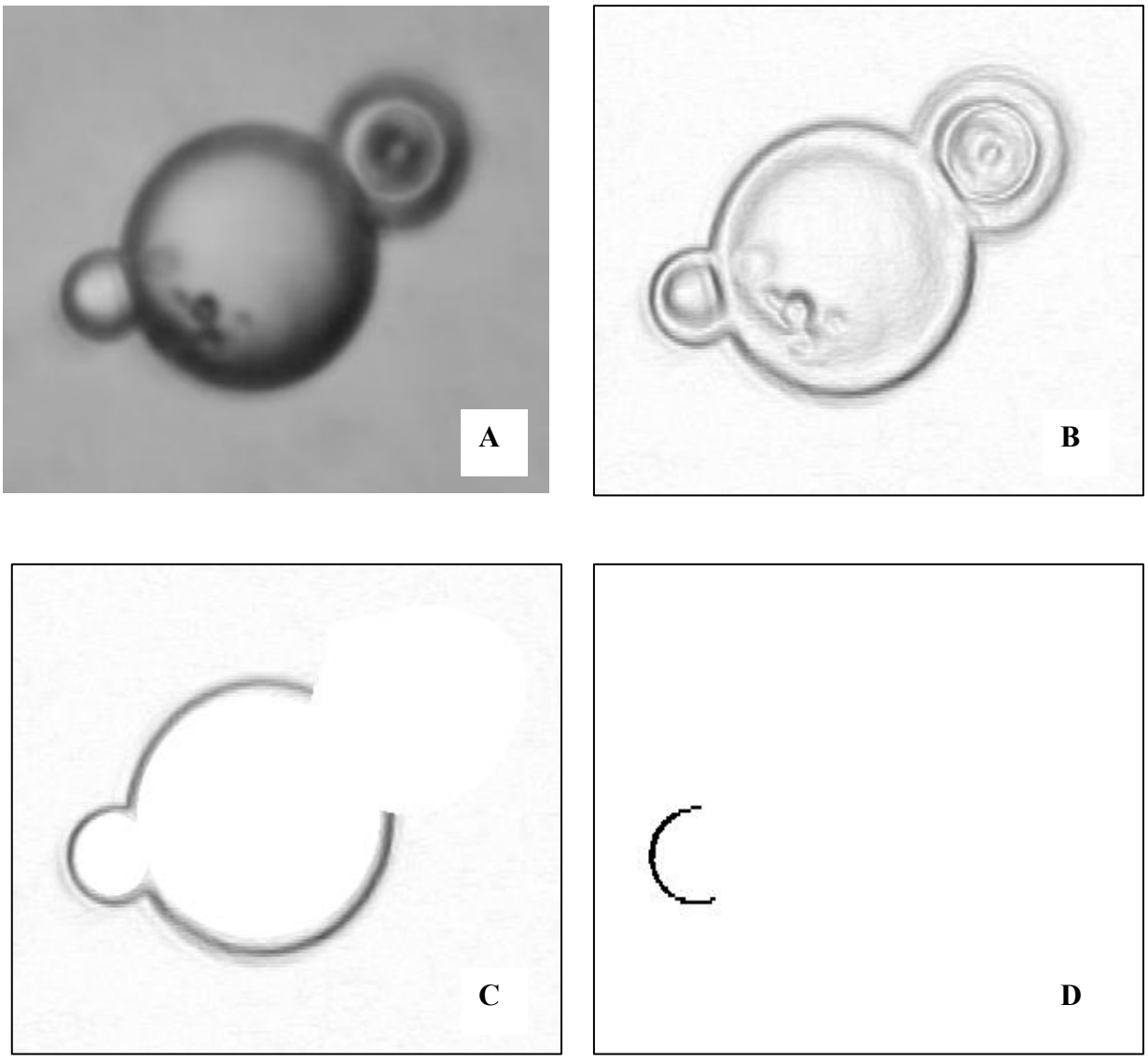

FIGURE 9 Stepwise method for bead radius determination. Raw image (*A),* note that bead pairing of interest is the large middle bead and the smaller bead on the left. (*B)* Image processed using "Find Edges" plug-in from ImageJ. (*C)* Cropping to get rid of unwanted bead and all image information not pertaining to the edge of the radius. (*D)* Separating the beads and thresholding the edge. Once the edge is thresholded, the X and Y coordinated for each pixel are compared to each other to calculate the curve and radius of bead.

smaller bead is free to float in the buffer. All the DNA bead preps are in a low salt buffer consisting of 0.1 M KCl, 0.02 M imidazole, and 5 mM $MgCl_2$ at a pH of 7. In this experiment, ds DNA is stretched parallel to its double helix. The slide is staged, and the 25X objective lens is used to find a potential bead pair. Of course some "pairs" might just be two uncoupled beads simply sitting next to each other on the slide. Before the GFS is put through its special orientation depending on the location of the floating bead in relation to the anchored bead, it is necessary to go through the plane of focus to determine if the small bead is not just sitting next to the large bead on the slide. Once it is determined that the small bead is attached, the GFS can be laid on its appropriate side and leveled. Each 600-frame movie is shot and archived, and the angle is sequentially advanced up or down by 2.5^0 depending on the relative position of the floating bead to the anchored bead on the monitor. This is repeated until the GFS has gone through an arc to capture the bead pair's d_{max} and d_{min}. Theoretically, there should be two d_{min} at angle α around 12.5^o symmetrically on either side of a centered d_{max} at α 0^o where the floating bead, the molecule, and the large bead line up pointed straight at the center of Earth's gravity.

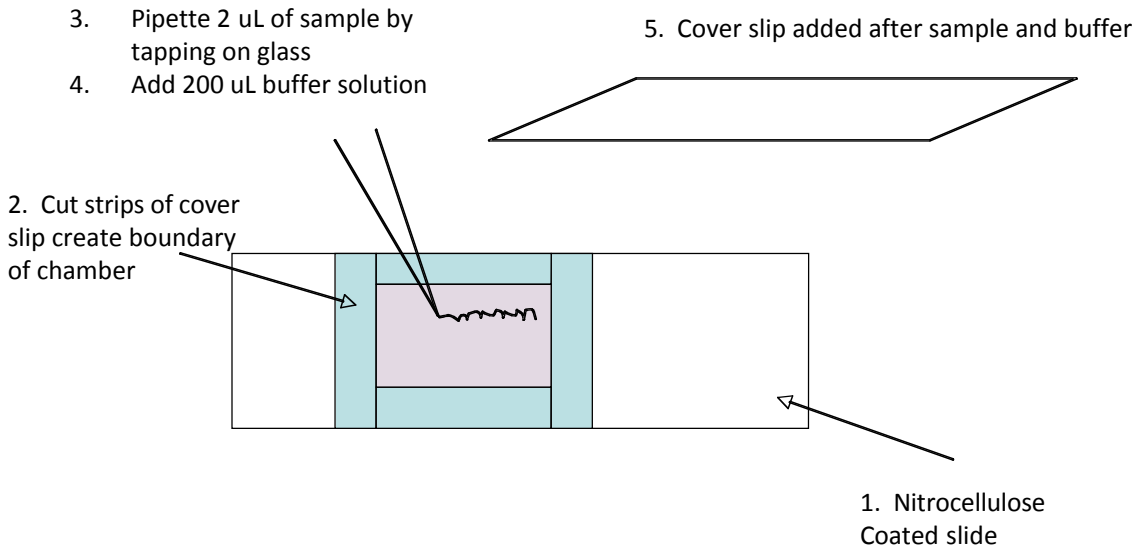

FIGURE 10 Sealed flow chamber assembly.

2.5 Parallel Stretch of Myosin Rod

In the first series of myosin experiments, the force is applied parallel to the rod. Additionally, a smaller batch of beads was used with larger beads. Another variation from the first protocol is the high salt buffer used in the chamber. This is a pH 7.0 buffer prepared with 0.5 M KCl, 0.02 M imidazole, and 5mM $MgCl_2$. A bead prep using the smaller 3-10 micron diameter beads were prepared with the MF30 antibody that attaches near the S1 head. These smaller beads were also labeled with rhodamine in an attempt to track the bead pairings. The larger beads (10-30 μm) were labeled with flouroscien and coupled with the MF20 antibody that attaches near the LMM of the myosin. This does ensure that proper bead pairings would have both attachment sites, which corresponds to the floating bead pulling against the length of the rod. These smaller beads impart forces including the expected range for single molecule forces involved in the powerstroke. Once those beads were analyzed, another batch was prepared using only large beads. This was an attempt to get a larger force range and maybe record a rupture force. It is worth noting that the dimeric nature of myosin II and of the monoclonal antibodies used means that the attachments were either on the same strand of the dimer, or on different strands. Because the MF30 antibody is C-terminal to the S1/S2 hinge, this stretch is intended to stretch the S2/LMM hinge, which is the only hinge between the attachment sites. Also, this is the first experiment where the 20X Zeiss lens was used for its greater depth of field during video capture.

2.6 Perpendicular Stretch of Myosin Rod

In the third experiment, force was applied perpendicular to the coiled-coil. In other words, the beads were only prepared with the MF30 antibody. In this configuration, beads would pair with the S1 heads between them and as the GFS is oriented, the heads might pull

apart due to the rod melting or uncoiling under force. Both sized beads were used and the beads were also fluorescently labeled with rhodamine in one batch and fluoroscein in the other. In one of the last preps, the digital video camera was employed.

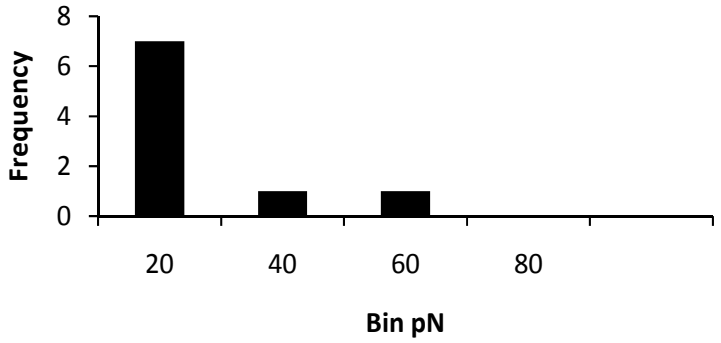

FIGURE 11 Histogram of 12 bp DNA implied rupture forces. Consistent with AFM measurements (Sattin et al., 2004), this short 12 bp hybridization appeared to be stable only up to about 20 pN of force in the gravitational force spectrometer.

TABLE 1 DNA force data

sample	pN
9	1.1652278
20	3.2421196
43	6.5119924
40	6.791719
53	10.064968
1	10.994139
42	18.070228
52	26.443575
2	57.900815

CHAPTER 3

RESULTS

3.1 DNA Control Results

The first experiment was designed as a control group to see if the gravitational force spectrometer (GFS) measurements were in line with previous work on DNA using Sattin's experimental AFM data. In the DNA control, nine samples out of 59 showed evidence of proper bead pairing. The other samples had too much noise to perform reliable analysis or were not properly paired to begin with. Of the nine working samples, eight of them support the idea that 12 bp DNA has a rupure force of approximately 20 pN as seen in Stattin's AFM study. The histogram in Figure 11 illustrates this. One sample reports a force of 57.9 pN, which corresponds to a floating bead radius of 9.8 microns, which is large for a floating bead. The approximate length of 12 bp DNA is 5 nm, which is well below the error of the GFS for this experiment. Our distance measurements, therefore, suffer from too much noise and are not reliable.

3.2 Results of Parallel Stretch

The second experiment introduces rabbit skeletal muscle myosin to the GFS. In this experiment, the force is applied parallel to the S2 by attaching the beads to the opposite ends of the subfragment. Of the 99 samples, 15 were analyzable. This data shows a range of lengths for S2 from 62 nm to 110 nm. Forces range from 0.13 pN to 88 pN. There are three discrete force ranges including the subpiconewton measurements, from 1.08-5.6 pN, and from 17.2-88 pN. We see that at the physiological force range (the second), the standard deviation of the distances is 18.3 compared to 14.5 for the subpiconewton group and 14.0 for the high force group. This is not a significant difference. The overall trend is that distance grouping appears to tighten as force is increased. To achieve a broad force range, the first half of this experiment uses the

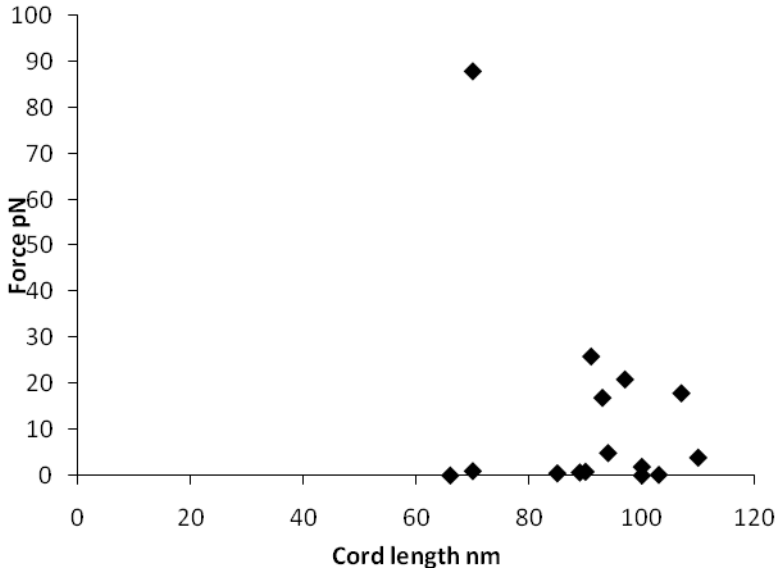

FIGURE 12 Force distance graph for S1-S2 parallel stretch.
Each point is the measured cord length for each myosin sample.
Note: three discrete force ranges.

TABLE 2 Summary of parallel stretch data from experiment 2

Mean cord length	91nm
SD	13.4 nm

smaller floating beads (3-10 um diameter) and the second half uses the larger floating beads (10-30 um diameter). It is important to note that the possible bead pairings include head-tail on the same strand in the myosin dimer; head-tail on opposite strands of the dimer; and less likely is the head-head attachment. To address this, the separate bead batches were fluorescently labeled with either fluoroscein or rhodamine. It proved impractical to verify the bead orientations with confocal microscopy because of issues of repeatability finding the same bead pair measured by the GFS. The new digital video camera is sensitive enough to record the fluorescence with the proper laser eliminating the need to lose and find the sample again on a different instrument at a different location. During this second experimental set up, a change to the thresholding technique was employed. This entailed setting the threshold for each movie based on the volume information from the last movie. This was done in an attempt to minimize the drift that had been occurring and rendering some data un-analyzable. The results for the different threshold techniques are given in Figure 13 and table 3.

3.3 Results of Perpendicular Stretch

The third protocol is designed to pull the dimer apart near the S1/S2 hinge region. Only the MF30 antibody is coupled to microspheres, which permit only bead pairings with both heads of the dimer in between. Of the fifteen samples, seven were analyzable and the last sample was recorded with the digital video camera. The data is plotted in Figure 14 in a force distance curve. The curve exhibits remarkable order for biological samples. All of the data was analyzed using the newer threshold technique.

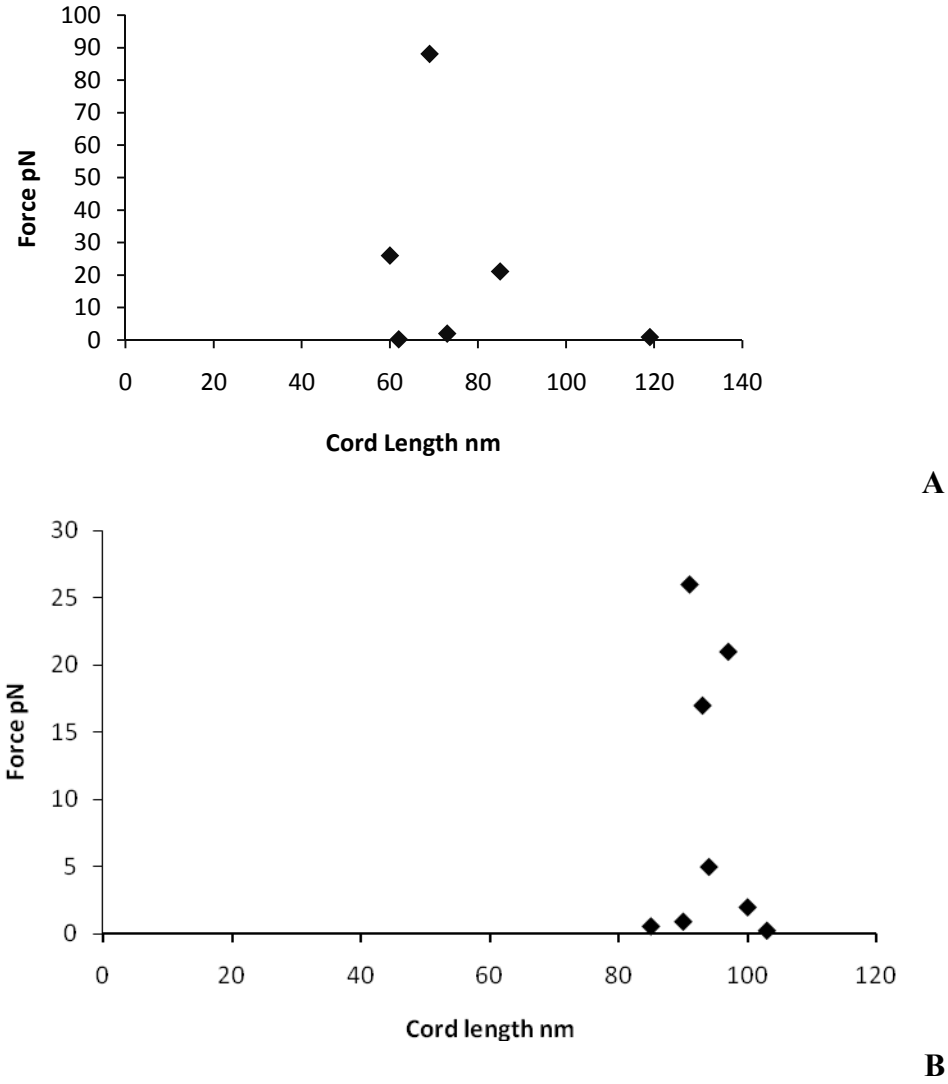

FIGURE 13 Old versus new threshold technique on parallel stretch data. (*A)* Old threshold technique on parallel stretch data. (*B)* New threshold technique on parallel stretch data, three points previously un-analyzable emerge with new technique. The mean molecular length for all forces was 94 nm with a standard deviation of 5.7 nm.

TABLE 3 Old versus new distance data

Sample	Old d nm	New d nm
77*	na	93
78*	na	95
17*	na	85
18	62	108
24	119	90
92	73	100
76	85	97
89	60	91
85	69	na
Average	78.0 nm	94nm
SD	22.0 nm	5.7 nm

* Indicates previously non-analyzable samples that emerged with new technique.

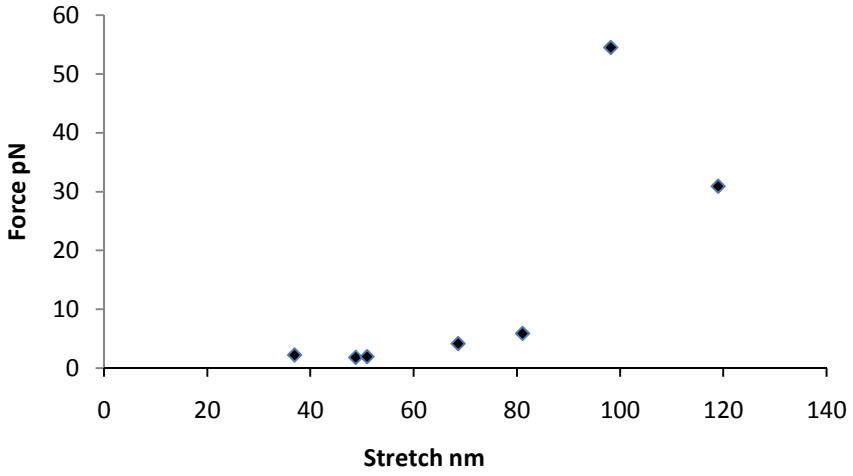

FIGURE 14 Force distance curve of perpendicular stretch data. Gravitational force spectroscopy of a single myosin dimer attached between two MF20 monoclonal antibodies that target each strand of the coiled coil near the S1/S2 hinge. See Figure 2 for reference.

TABLE 4 S1/S1 Perpendicular Stretch Data

Myosin sample	Stretch length nm	Force pN
103	48.8	1.83
110	51.0	1.96
108	36.9	2.24
102	68.6	4.17
107	81.1	5.90
109	98.2	54.5
115	119.0	30.92

CHAPTER 4

DISCUSSION

4.1 Agreement with Previous Force Data on 12 bp DNA

These experiments were done with novice lab technique including problems focusing the image and maintaining a constant focus on the image. The gravitational force spectrometer (GFS) also showed a tendency to image beads with a thickening on one side or the other of the outline of the beads. This throws off the centroid analysis. After several runs, it was determined that the diaphragm was not properly aligned. The binary images after thresholding also retained a tendency to drift throughout a measurement. This made many samples too noisy to analyze. As a result, the 22 nm error in the GFS's distance measurements was too much to accurately describe the 5 nm length of 12 bp DNA. The characteristic curve of d_{min} to d_{max} to d_{min} was being obscured by wild threshold fluctuations in many cases. Preliminarily, improvements in focusing yielded more consistent results although the major breakthrough came in the perpendicular stretch experiments using rabbit skeletal myosin. The first wave of sealed chambers where the sample is placed often lost their seals quickly and intruding air bubbles rendered the sample useless. This was corrected with patience and improving the construction of the sealed chambers.

While the distance measurements are unreliable, the force measurements are precise. The reported rupture force of the double helix is approximately 20 pN for 12 bp ds DNA according to calibrated experiments using AFM in the Sattin lab. All but one GFS result is in this range. This is significant because it shows agreement and repeatability with a completely different experiment using fundamentally different equipment. Also, this reveals one of the best qualities of the GFS, which is its ability to calibrate itself as long as the investigator is working with the

earth's gravity. AFM requires intense attention to the experimental conditions including the buffer, the spring tension of the cantilever arm, the cleanliness of the surface and the type of surface. While all these can be accurately accounted for per experiment, it is much more difficult if not impractical to attain exact condition from experiment to experiment or from instrument to instrument. The idea is not to replace AFM or any other useful instrument, but to compliment the field of structural biochemistry. The GFS is inexpensive, needs no calibration, and can resolve forces on the order of hundredths of piconewtons. It does not have the distance resolution of the AFM but is much more capable of imparting loads in the physiological force range than any instrument available. Because of the successful results regarding rupture force of 12 bp DNA, the experiments on myosin were carried out with confidence.

4.2 Discussion of Parallel Stretch

In the first experimental group, rabbit skeletal myosin was tethered between a large and small bead. The first obvious observation in this assay was the visually alive looking floating beads dancing around their anchored partners. There are two reasons for this. First, the length of S2 is approximately twice that of the 12 bp DNA, and the smaller beads allowed greater degrees of freedom around the attachment points. Later controls reproduced these visual results. Another possibility, which also yielded similar results were when a low salt buffer was used instead of the high salt buffer. This allowed for the possibility of the myosin to form into its native filamentous state thus becoming much longer. This visual cue reaffirmed that the pairings were indeed taking place, although with larger floating beads, the degrees of freedom were lost and a more static image once again emerged.

The results plotted in Figure 12 show an overall trend. This is as force increases, a tightening of the data seems apparent. Actually, there are three distinct groups based on their

force ranges. There are the subpiconewton group, the physiological force range from 1-5.6 pN and the higher forces up to around 60 pN. While not statistically significant, the standard deviation of the middle physiologically relevant group was larger than the two groups on the extremities of the spectrum. This might lead future studies into signal transduction of physiological forces on single molecules. In fact, it has been reported that myosin 1 can act as a force sensor (Laakso, Lewis et al., 2008). While myosin 1 is very different than myosin 2, there might be a conserved force sensor in S1 in both isoforms. Perhaps the coiled-coil under physiological force tends to melt more readily and become more flexible giving a greater variance in distance measurements.

Initially, I expected to see the length of the rod increase with increased force. Hypothetically, the S2/LMM hinge ought to stretch as force is applied. This is because the beads are tethered to MF20 and MF30, so the S1/S2 hinge is left out. This is simply not the case as distance measurements for S2 in this assay range from 65-110 nm. However, this does not preclude the hypothesis that graded resistance should lengthen the sample. One would expect to see around 10 nm of stretching at the higher force range. The overall error in experiment 2 including all data was about 14 nm after the data were optimized with the new threshold method, so the test was not sensitive enough to determine if the stretch is actually occurring or not. Another reason for this is the bead pairing orientation for each sample. The solution is to label the different bead preps that correspond to different antibodies and look at the bead pairings with a fluorescent scope. This was tried several times, however, there was never a good way to find the same bead pair on two different instruments, often housed in different locations. Another problem might have been the labeling efficiency, which was not measured. It is worth noting, however, that because of available degrees of freedom in binding, most pairings should have

been head to tail as it is harder to get two beads binding both at the head region. In any event, the data leaves us with a little mystery, but measures can be taken in the future to ensure the investigators know the orientations of the bead pairings. Mainly, fluorescent labels on the beads can confirm orientation and this is made easier with the advent of the more sensitive digital video camera added to the GFS.

It is also possible that the overall trend is misleading from a standpoint of selection bias. Working with the GFS, it becomes obvious that most good pairings involve pairs where the floating bead is significantly smaller than the larger anchored bead. Experimentally, it would be difficult to find a proper pair of the same sized bead, for the pair would tend to stack on the glass slide together. Also, there is a selection bias against very large floating beads because determining their status in a pair becomes more difficult when there is not some discrepancy in the plane of focus from one bead to another. A larger sample size would probably address this concern. Also, all measurements should now be done with the more sensitive digital video camera in conjunction with the new thresholding method. There is no reason to believe that the limits of resolution have been reached at this stage.

4.3 Discussion of Perpendicular Stretch

In a study using fluorescent resonance energy transfer (FRET), evidence suggesting the dimer does not uncoil while both S1 heads are bound to actin in a post-powerstroke state was presented (Chakrabarty, Xiao et al., 2002). Indeed there are those who support the idea that the myosin step can be accounted for by bending in the light chain domain (Molloy, Kendrick-Jones et al., 2000). However, the perpendicular stretching of S2, the results indicate that the dimer can be pulled apart with increasing force, and that as the dimer is pulled apart, it becomes less stable. Otherwise, the graph would not show a textbook relationship between force and overall length.

This is significant, for it is the first time structural evidence has been presented that shows vertebrate skeletal muscle can undergo such a process. It has been supposed before that as melting of the coiled-coil occurs; the individual α helices revert to random coils (Gundapaneni, 2004). These random coils have less torsional rigidity thus more flexibility. It is also thought that the hinges are random coil and this conformation is the reason for the increased flexibility. The force distance curve in Figure 14 shows the melting of the dimer effectively produces an elongated hinge structure loosing stability as the dimer unwinds. According to my hypothesis, the dimer melts and the individual α helices separate. As they do, the tertiary structure that stabilizes them becomes less influential and the α helix reverts to a random coil conformation. The force transmitted along the rod could act as a signal for the hinge to open and the dimer to uncoil, or the force could directly cause the structural melt. These ideas need to be investigated, and the GFS would be a likely candidate to perform such assays. Another question about the mechanism of refolding is pertinent here. This might be an exquisitely regulated process, or it could be a function of kinetics, or recoiling as the result of a build-up of torque at the S2/LMM hinge. Remember that *in vivo*, the rod is attached to the LMM. If the dimer is melting at S2 while both heads of S1 are attached to actin, then it is concentrating a supercoiling event somewhere down line because the LMM is anchored to the rest of the thick filament. An assay using the basis of experiment 3 could be modified where we label the LMM with fluorescent probes and monitor it to see if it spins as force is applied perpendicular to the rod as in experiment 3.

Looking at the force distance curve from the data generated in Figure 14, it is clear that the myosin heads are separating in a force dependant manner. While more data needs to be acquired to give a more perfect picture, it is tantalizing to speculate about the nature of this data.

For instance, if the data was fitted to a worm-like chain model (WLC), might this model give us useful information by which to make meaningful predictions? The WLC is used to as to describe unstable molecules or areas of molecules. Simply, the least stable region in the chain stretches from a random coil to something like a β sheet and this region elongates first. Then the next weakest link undergoes conformational change and elongation and so on. The flexible nature of the S1/S2 hinge makes it a candidate for WLC modeling, and this idea might be reinforced in light of the force dependant nature of the S1-S1 stretch data. If the data sufficiently fit the model, we can accurately predict the number of amino acid residues that are participating in an uncoiling event. This is a far more robust way of considering the flexibility of S2 because it provides a framework by which to compare other isoforms of myosin II, including mutant variants. This might prove vital for elucidating the molecular mechanism of HCM.

4.4 Improvements to Video System

Virtually all of the data collected and analyzed used the analog video system. However, there has been an upgrade in the form of a Sony digital video camera. Digital video has several characteristics that set it apart from analog video. Instead of archiving with videotape, the data from the digital video camera is stored in an external hard drive. Also, because of its digital nature and its requirement for system memory to run at optimum speeds, the frame rate is variable when compared to analog video, which is extremely precise regarding frame rate. However, when the initial settings are optimized, the digital camera can acquire images routinely at 90 frames per second and sometimes as high as 450 frames per second. This could be useful when doing time-based calculations such as fast Fourier transformation. Alternatively, the system can be set up to run at slower frame rates to maximize resolution. The digital image is noticeably cleaner and does not need to be optimized or deinterlaced before it is put into binary

images, and this results in finer binning which could lead to even better distance measurement resolution than the current 5.7 nm with the analog video system. Another advantage of moving toward digital video is that the information is always in the digital domain and therefore does not need to be converted. The camera runs directly into an Intel Core 2 duo processor via a fire wire port where the movies are primed for digital manipulation via ImageJ. The improved camera is also sensitive enough to utilize fluorescence of dyes under laser light. This could be very useful when determining true bead pairings or the nature of the bead pairing.

4.5 Improvements to Threshold Technique

The single most significant improvement to the GFS system was in the thresholding technique. The process of setting the threshold or converting the video into a binary image has always been crucial for accurate measurements. The centroid analysis (and ultimately the distance measurement of S2) depends on obtaining the X and Y values of the center of the bead's image. Those values are determined using the inside edges of the image. If the focus is held constant from the microscope, then there is a better chance of getting consistent values when setting the threshold. However, the actual sample is moving in space between every movie, so there is always some degree of floating or error. Visually, there are often subtle changes in those inside edges over the course of some 20 movies all at different spatial orientations regardless of how carefully maintained the focus is at the microscope. Also, the beads are not in the exact plane of focus because they are different sizes and also have their own independent spatial relationships throughout an entire series of measurements. So, every variation in one bead is not necessarily translated in the other bead of the pair. This means that one bead could have a minor variation in the location of its inside edge in threshold, meaning the outline of the bead is slightly thicker which corresponds to less volume inside the bead and a possible different X, Y

coordinate for its centroid position. Because the other bead in the pair is not in the exact plane of focus as the first because of their size discrepancies, which can be large or small, disproportionate thickening or thinning can happen simultaneously causing its centroid position to float. If the "float" was exactly the same for both beads, there would be no issue, but the observations do not support such a scenario. Upon gaining this insight into the nature of the GFS, it became apparent that to ultimately achieve better distance resolution, the threshold must be adjusted to obtain consistent inner volumes of the beads from movie to movie. Also, in line with this idea, is to maintain independent threshold values for each bead instead of simply setting the limit for both. This latter practice had been adopted earlier in the second protocol, but it was not clear it was a better practice as those final results contained similar measurement error of around 20 nm. However, when combining the independent thresholds with the practice of adjusting the threshold for each movie, the error was reduced to approximately 5.7 nm. Table 3 shows "old" and "new" distance measurements of bead pairs that were initially analyzed with the original or old technique and subsequently with the improved technique. Not every bead pair benefited from re-analysis, but the results were so convincing that every pair from that point uses the improved technique for better accuracy. There is one advantage of the first technique in automating the system for speed, but it is clear at this time that gaining a fourfold increase in resolution is more productive for this type of nano-scale measurement.

4.6 Other Improvements

The first improvement to the developing GFS I made was a simple one. Originally, the instrument employed the use of a large clamp to immobilize the head where the eyepiece resides. On a normal microscope, this feature is to allow rotation of the head. In our configuration, this was not desirable. I aligned the head and glued it with a strong epoxy. This stabilized the

region, and because the clamp was no longer present, the GFS could attain more degrees of freedom before bumping into its mount. This allows more bead pairings to be analyzed.

One idea was to use a θ stage with clips. The idea was to find a proper bead pair and to manually put it into an orientation where the GFS would only go through one consistent range of motion as opposed to a different one on most runs. It quickly became apparent that the fine muscle movement needed to manipulate these small arrangements was too difficult for me. I reverted back to the adjustable stage.

One of the best improvements was the use of the Zeiss 20X lens. This lens has less resolving power than the others in the GFS, but it is this relationship between resolution and field of view that made it invaluable. Because the field of view increased, both beads in the pair tended to stay in focus over the course of the entire measurement. This led to better and more accurate distance measurements and made many samples viable for analyzing. For instance, if the discrepancy between bead sizes in a pair is great, than one or the other is more likely to go out of focus because they do not share the exact same plane of focus. This is especially true in the GFS system where the sample is moved in space at least 20 different times. However, when the field of view is increased, the effective plane of focus increases as well and bead pairings of different sizes appear stable over the course of a measurement.

For a time, emphasis was put on automating the system. While this is still something desirable, for the time being, it has been discarded in favor of the independent threshold system that yields far more accurate distance measurements. During the automation process, many useful plug-ins were developed that can be employed at a later time. These would set the threshold automatically, analyze the centroid and dump the data into Excel. The main advantage of this process was that it cut the analysis time down considerably. However, when the

independent threshold technique was refined, it could not be automated easily. In the pursuit of the highest accuracy, automation was shelved. This is significant, for if we had proceeded with automation instead of independent thresholding, I doubt the clean data would have emerged for the S1/S1 perpendicular stretch.

One very useful advance was to smooth the individual distance measurements in Excel. Each frame of video yields a distance measurement for the length between the centroids of the beads in microns. A rolling average was constructed in the spreadsheet that averaged every fifteen measurements. This increased the length of the movie to get 630 frames instead of only 600. The result was finer binning which leads to a more accurate final cord length. Samples that underwent smoothing fit the model with less nudging. The error was reduced by a small but significant percent. In comparison to independent thresholding, smoothing is a minor advance. Still, when trying to resolve on a nanometer scale, every improvement is important.

When adding myosin to glass beads it is important to agitate the mixture so a maximum of binding occurs. One problem early on was the myosin's tendency to irreversibly clump up upon agitation, which rendered the mixture useless. A table-top rotator was used to fix this, and it did help the clumping. However, the feeling was that the mixture was not being agitated enough to maximize pairing. To deal with this, I removed the clear cover from the face of a standard wall clock to expose the hands. I attached the top of the microcentrifuge tube to the axis of the second hand and plugged in the clock. This resulted in a slow rotator with a cycle of exactly one revolution per minute. This also optimized bead mixing without having to resort to doing it by hand.

Another improvement to the protocol came in the assembly of the sealed chamber where the sample is held. Originally, glass strips were cut, and vacuum grease decanted by a syringe to

seal the strips to the glass slide. This usually resulted in a chamber that was leaky. A leaky chamber would spell the premature and swift demise of the sample, and this could come about at any time. This was not helpful while doing experiments where the loss of the seal means the end of the experiment and the building of a new cell. My solution was two fold. First, I only use the factory edge of cover slips to create the interior boundary of the chamber. Secondly, instead of using the syringe, I rake the strips across a palette of grease to give a nice uniform bead. This is done to both sides of the strips so it seals to the slide and to the final cover slip that holds the buffer and sample in. Now, my chambers hold a seal for up to a year with the wet sample inside. This is far longer than is useful for these experiments but it does eliminate the problem of drying out mid-experiment.

The last minor improvement was employing the use of an air table. The GFS is mounted to an air table and the table absorbs shock. This is useful for reducing noise on the video acquisition. The distance measurements provide for tighter binning and ultimately a more accurate cord length. This was less of an improvement and more of an observation that our table was not working. It had always been part of the design to use the table, but because it had no pressure, the shocks from the experiment were not being absorbed. A quick call to maintenance fixed this. This was not a trivial improvement as it was as useful as the data smoothing as far as getting tighter bins. The move to the digital video camera provides the most noticeable effect on the bins by comparison.

4.7 Speculation on Future Assays

This study has established some unique characteristics of a novel instrument. It is useful to think about the immediate future and to speculate on the kinds of investigations the GFS might be capable of. In the near future, it would be a good idea to really push the limits of the system.

For instance, there is a user selection bias against using large floating beads because they are so similar in size to their anchored counterparts that their planes of focus are often the same. In this way, there is no preliminary way to determine if they are actually paired. To get force data in the hundreds of piconewtons, these suspect bead pairs must be analyzed. One way to overcome the bias is to re-implement the practice of using different colored beads. With the addition of the digital video camera, there should be enough information to determine the nature of true bead pairings without having to travel to a different facility and use a different instrument. So, the bottom of the force spectrum the GFS is capable of is better defined, and the larger forces should be explored. This would especially help order the data from any future stretching of myosins that direct the force parallel to the coiled-coil similar to experiment 2. Doing this would give greater depth to the data already collected. Eventually, GFS stretch data could be incorporated to more sophisticated computer algorithms for accurate modeling purposes.

The next logical step after gathering a suitable depth of data on the wild-type would be to stretch mutated myosins. Obtaining available myosin mutants and approaching the GFS with a shotgun methodology could do this. This would eventually create a "stretch databank." Otherwise, it would be directly useful to obtain myosin with the same mutations that have already been modeled in our unpublished data, or myosins mutated in the same ways that are presented in clinical studies. For instance, if normal myosin II stretches in the characteristic way it does in experiment 3, what does the stretch profile look like if you use a deletion or missense mutation in the S1/S2 hinge region? It has been reported that some myosin mutations implicated in HCM actually increase myosin function. In other words, some mutants can translate actin with more speed and force than wild-type (Dantzig, Liu et al., 2006). It would be interesting to see the stretch profiles of different mutants to wild-type. The data from GFS would hone the

biological hypotheses that explain HCM. Do different types of mutations within species give different stretch profiles? If flexibility is altered with different mutants, our study could be useful.

As a new instrument, the GFS is subject to many kinds of modification. It would be easy to modify the system to study different variables on whatever molecule is chosen. For instance, temperature could be held constant or varied. This could bridge the gap between thermodynamic studies and force studies which both deal with melting of supercoils. A similar assay could be constructed with the GFS and data could be compared to thermodynamic stability studies. Each force group could be subjected to discrete temperatures to see if there is an agreement with previous work looking at thermodynamically stable range of temperatures on a coiled-coil. In other words, as the temperature rises, is it easier to pull the myosin dimer apart? This type of data could also be applied to any mutant studies.

The sealed chamber, and the sample that is mounted onto the stage of the GFS is not dissimilar from flow cells in single molecule motility assays. The chamber could be modified in a way that reagents could be introduced to the sample at desired times. For instance, a molecule of myosin could be stretched at d_{max} at equilibrium and recorded. Then, while still under force, ADP could be added to the chamber in a way to induce rigor. The length of S2 and its hinges could be measured in before and after states and the distance of the shortening, if any, could be compared to existing data regarding the powerstroke. This might or might not shed further light on the nature of S2's flexibility in the context of muscle contraction. This could be made more viable by automating the system, which would require some computer programming. An automated system would have a continuous video feed and dynamics could be measure in real time.

One of the main advantages of the GFS is its low cost of operation and care. If one were to design a version without cost in mind, a very sophisticated instrument could be presented. My ultimate vision for the GFS is a fully automated spinning disk confocal microscope mounted on a fully mechanized stage. The light source could be fed into the system with flexible fiber optics. This way, small fluors like quantum dots or GFPs could be attached to the same antibodies that are directed at specific sites. This version could still use microspheres as a way of imparting force, but eliminates the need to evaluate the beads' centroid. Instead, the centroid positions of the quantum dots attached at specific sites could be determined and the resolution of the distance measurements could potentially move into the angstrom range as there is not a substantial theoretical limit to the distance resolution. As long as cost is no object in this speculation, the anchored bead could be substituted for a nanotube running parallel with the slide. The floating beads would be attached to the tube. This could eliminate the need for a fully rotatable stage in favor of a permanent stage set at 90^{o}. Then the chamber containing the nanotube and the tethered microspheres is placed on the microscope stage and all the beads are already at d_{max} and a simple measurement can be taken. In any event, the use of gravity to stretch filamentous macromolecules like myosin, nebulin, or titin can be expounded upon in many directions.

4.8 Conclusions

The GFS is a powerful instrument capable of precise measurements both in force and displacement. It should be added to the roster of capable systems, each with their own advantages and limitations to do single molecule force assays. Even in a primitive state, the GFS has shed light on the structural nature of dimeric S2. While developing the instrument, several improvements were made. Most were small and helpful, but the breakthrough in the threshold technique cut the error rate four fold. This refinement made it possible to accurately observe the

uncoiling of the myosin dimer at low forces. This led to new direct structural evidence that the rod can indeed confer flexibility to the molecule. While the total nature of the flexibility has not been elucidated, the direction is clear. At physiological forces, the dimer is capable of unwinding in relation to the load imparted to it. This study is the first to demonstrate that myosin II is capable of uncoiling under physiological force loads. This is similar to the observed melting of the analogous subunit of non-muscle myosin VI. However, the process is for a different purpose in contractile proteins. This flexibility that allows processive motors to take step size longer than their primary structure would allow might be the same process that confers the necessary flexibility for S1 to bind to actin with a working distance of 19 nm in a pre-powerstroke conformation. Furthermore, the activity infers previously unknown qualities of the structure and function of the rod. This is a unique characteristic in a universe of protein diversity. It is reasonable to speculate that mutations structurally affecting this unique function can ultimately lead to the disease state. It is therefore clinically important to continue to illuminate the role of S2's reported flexibility in context of muscle contraction. HCM is caused by one of over 200 mutations to the sarcomeric proteins.

It is reasonable to think that a mutation to S2 or its hinges might cause a loss or gain of flexibility that can lead to an overstressed cardiac muscle that over time becomes diseased. It is clear from the data in the S1/S1 stretch experiment that the WT skeletal S1/S2 hinge can readily come apart at or near physiological force loads. How might the force distance curves from mutated S2 look in comparison to WT force distance curves? If the hinge regions can't melt or if the dimer itself remains rigid, the degrees of freedom needed to absorb powerstroke are reduced. Alternatively, the mutant might become too flexible or unstable. In this scenario, coordination of the S2 could be lost and this might be the mechanism that leads to pathogenesis. In either case,

the heart is over-worked in response to reduced blood volume per pump. This thickens the left ventricle and the heart loses symmetry. In this mutated configuration, it is only a matter of time before the out-of-balance system begins to deteriorate leading to a bad outcome such as sudden death. If my hypothesis is true, then it is imperative to continue the structural work on the sarcomeric proteins to accurately describe their normal structure and function. This is to be compared to the structural differences in mutated forms which lead to altered function. Single force assays are one way to study these nuances and the GFS has the sensitivity and accuracy to do these analyses.

One of the most compelling ideas that this type of study points to involves signal transduction. If indeed, the S2 dimer coils and uncoils under load to accommodate muscle myosin's total function, then there is a signal, a signal path and there is regulation of the signal. Studies have, on the periphery, alluded to the idea that there might be force sensors in the sarcomeric proteins (Petrofsky and Phillips, 1985; Le Guennec, Cazorla et al., 2000). In an unpublished paper, Puchner uses AFM to test if titin kinase is a force sensor. Because of the forces involved, the GFS might be a prime candidate for similar assays. Evidence from OT assay shows that a single point mutation in the SH-1 domain of non-muscle myosin 2 leads to instability of the dimer, a loss of flexibility, and a loss of motile function (Iwai, Hanamoto et al., 2006). This implies that the myosin head itself might be used as a force sensor that transmits information down line. This might only occur in a physiologically relevant force range like the range available from GFS. Repeating these types of experiments with the GFS is a real option that might lead to further understanding of signal transduction. While this is speculative, there is no doubt that being able to manipulate signals could potentially solve very old and difficult clinical problems including but certainly not limited to HCM.

REFERENCES

Adamovic, I., S. M. Mijailovich and M. Karplus. 2008. The elastic properties of the structurally characterized myosin II S2 subdomain: a molecular dynamics and normal mode analysis. *Biophys J.* 94:3779-3789.

Beausang, J. F., H. W. Schroeder, 3rd, P. C. Nelson and Y. E. Goldman. 2008. Twirling of actin by myosins II and V observed via polarized TIRF in a modified gliding assay. *Biophys J.* 95:5820-5831.

Castro-Zena, Pilar C. 2007. Hindrance of the myosin power stroke posed by the proximity to the troponin complex identified using a novel LRET fluorescent nanocircuit. Masters thesis, University of North Texas, Denton.

Chakrabarty, T., M. Xiao, R. Cooke and P. R. Selvin. 2002. Holding two heads together: stability of the myosin II rod measured by resonance energy transfer between the heads. *Proc Natl Acad Sci USA.* 99:6011-6016.

Cuda, G., L. Fananapazir, N. D. Epstein and J. R. Sellers. 1997. The in vitro motility activity of beta-cardiac myosin depends on the nature of the beta-myosin heavy chain gene mutation in hypertrophic cardiomyopathy. *J Muscle Res Cell Motil.* 18:275-283.

Cuda, G., L. Fananapazir, W. S. Zhu, J. R. Sellers and N. D. Epstein. 1993. Skeletal muscle expression and abnormal function of beta-myosin in hypertrophic cardiomyopathy. *J Clin Invest.* 91:2861-2865.

Dantzig, J. A., T. Y. Liu and Y. E. Goldman. 2006. Functional studies of individual myosin molecules. *Ann N Y Acad Sci.* 1080:1-18.

Debold, E. P., J. P. Schmitt, J. B. Patlak, S. E. Beck, J. R. Moore, J. G. Seidman, C. Seidman and D. M. Warshaw. 2007. Hypertrophic and dilated cardiomyopathy mutations differentially affect the molecular force generation of mouse alpha-cardiac myosin in the laser trap assay. *Am J Physiol Heart Circ Physiol.* 293:284-291.

Epstein, N. D., G. M. Cohn, F. Cyran and L. Fananapazir. 1992. Differences in clinical expression of hypertrophic cardiomyopathy associated with two distinct mutations in the beta-myosin heavy chain gene. A 908Leu----Val mutation and a 403Arg----Gln mutation. *Circulation.* 86:345-352.

Georgakopoulos, D. and V. Tolis. 2007. Hypertrophic cardiomyopathy in children, teenagers and young adults. *Hellenic J Cardiol.* 48:228-233.

Gruen, M. and M. Gautel. 1999. Mutations in beta-myosin S2 that cause familial hypertrophic cardiomyopathy (FHC) abolish the interaction with the regulatory domain of myosin-binding protein-C. *J Mol Biol.* 286:933-949.

Gundapaneni, Deepika. 2004. Studies on actomyosin crossbridge flexibility using a new single molecule assay. Masters thesis, University of North Texas, Denton.

Harris, S. P., E. Rostkova, M. Gautel and R. L. Moss. 2004. Binding of myosin binding protein-C to myosin subfragment S2 affects contractility independent of a tether mechanism. *Circulation Research.* 95:930-936.

Huxley, A. F. and R. M. Simmons. 1971. Proposed mechanism of force generation in striated muscle. *Nature* 233:533-538.

Iwai, S., D. Hanamoto and S. Chaen. 2006. A point mutation in the SH1 helix alters elasticity and thermal stability of myosin II. *J Biol Chem.* 281:30736-30744.

Laakso, J. M., J. H. Lewis, H. Shuman and E. M. Ostap. 2008. Myosin I can act as a molecular force sensor. *Science.* 321:133-136.

Lauzon, A. M., P. M. Fagnant, D. M. Warshaw and K. M. Trybus. 2001. Coiled-coil unwinding at the smooth muscle myosin head-rod junction is required for optimal mechanical performance. *Biophys J.* 80:1900-1904.

Le Guennec, J. Y., O. Cazorla, A. Lacampagne and G. Vassort. 2000. Is titin the length sensor in cardiac muscle? Physiological and physiopathological perspectives. *Adv Exp Med Biol.* 481:337-351.

Maron, B. J. 2002. Hypertrophic cardiomyopathy: a systematic review. *JAMA.* 287:1308-1320.

Miyata, H., H. Yoshikawa, H. Hakozaki, N. Suzuki, T. Furuno, A. Ikegami, K. Kinosita, Jr., T. Nishizaka and S. Ishiwata. 1995. Mechanical measurements of single actomyosin motor force. *Biophys J.* 68:286S-290S.

Molloy, J. E., J. Kendrick-Jones, C. Veigel and R. T. Tregear. 2000. An unexpectedly large working stroke from chymotryptic fragments of myosin II. *FEBS Lett.* **480**:293-297.

Nabiev, S. R., D. A. Ovsiannikov, B. Bershitskii and S. Bershitskii. 2008. [Optical trap as a tool for studying motor proteins]. *Biofizika.* 53:929-35.

Nachmias, V. T. and H. E. Huxley. 1970. Electron microscope observations on actomyosin and actin preparations from Physarum polycephalum, and on their interaction with heavy meromyosin subfragment I from muscle myosin. *J Mol Biol.* 50:83-90.

Oota, S. and N. Saitou. 1999. Phylogenetic relationship of muscle tissues deduced from superimposition of gene trees. *Mol Biol Evol.* 16:856-867.

Petrofsky, J. S. and C. A. Phillips. 1985. Closed-loop control of movement of skeletal muscle. *Crit Rev Biomed Eng.* 13:35-96.

Rawlins, J., A. Bhan and S. Sharma. 2009. Left ventricular hypertrophy in athletes. *Eur J Echocardiogr.* 10:350-356.

Rock, R. S., S. E. Rice, A. L. Wells, T. J. Purcell, J. A. Spudich and H. L. Sweeney. 2001. Myosin VI is a processive motor with a large step size. *Proc Natl Acad Sci U S A.* 98:13655-13659.

Rock, R. S., M. Rief, A. D. Mehta and J. A. Spudich. 2000. In vitro assays of processive myosin motors. *Methods.* 22:373-381.

Root, D. D., S. Stewart and J. Xu. 2002. Dynamic docking of myosin and actin observed with resonance energy transfer. *Biochemistry.* 41:1786-1794.

Root, D. D., V. K. Yadavalli, J. G. Forbes and K. Wang. 2006. Coiled-coil nanomechanics and uncoiling and unfolding of the superhelix and alpha-helices of myosin. *Biophys J.* 90:2852-2866.

Sattin, B. D., A. E. Pelling and M. C. Goh. 2004. DNA base pair resolution by single molecule force spectroscopy. *Nucleic Acids.Res.* 32:4876-4883.

Shimizu, T., J. E. Dennis, T. Masaki and D. A. Fischman. 1985. Axial arrangement of the myosin rod in vertebrate thick filaments: immunoelectron microscopy with a monoclonal antibody to light meromyosin. *J Cell Biol.* 101:1115-1123.

Sugiura, S., N. Kobayakawa, S. Momomura, S. Chaen, M. Omata and H. Sugi. 1996. Different cardiac myosin isoforms exhibit equal force-generating ability in vitro. *Biochim Biophys Acta.* 1273:73-76.

van Dijk, S. Dooijes, D. dos Remedios, C. Michels, M. Lamers, J. Winegrad, S. Schlossarek, S. Carrier, L. ten Cate, F. Stienen, J. van der Velden, J. 2009. Cardiac myosin-binding protein C mutations and hypertrophic cardiomyopathy. *Molecular Cardiology.* 119:1473-1483.

Toyoshima, Y. Y. 1991. Bidirectional movement of actin filaments along tracks of heavy meromyosin and native thick filaments. *J Cell Sci Suppl.* 14:83-85.

Toyoshima, Y. Y. 1991. Flexibility in actin-myosin motility system revealed by in vitro motility assay. *Adv Biophys.* 27:213-220.

Toyoshima, Y. Y., S. J. Kron, E. M. McNally, K. R. Niebling, C. Toyoshima and J. A. Spudich. 1987. Myosin subfragment-1 is sufficient to move actin filaments in vitro. *Nature.* 328:536-539.

Toyoshima, Y. Y., S. J. Kron and J. A. Spudich. 1990. The myosin step size: measurement of the unit displacement per ATP hydrolyzed in an in vitro assay. *Proc Natl Acad Sci U S A.* 87:7130-7134.

Tyska, M. J., D. E. Dupuis, W. H. Guilford, J. B. Patlak, G. S. Waller, K. M. Trybus, D. M. Warshaw and S. Lowey. 1999. Two heads of myosin are better than one for generating force and motion. *Proc Natl Acad Sci U S A.* 96:4402-4407.

Weston, P. D. and S. Avrameas. 1971. Proteins coupled to polyacrylamide beads using glutaraldehyde. *Biochem Biophys Res Commun.* 45:1574-1580.

Zhang, H. and K. K. Liu. 2008. Optical tweezers for single cells. *J R Soc Interface.* 5:671-690.